

**UNDERSTANDING THE IMPACT OF LIGNIN-DERIVABLE NON-
ISOCYANATE POLYURETHANE (NIPU) CHEMISTRY ON
ELECTROSPINNABILITY AND FIBER QUALITY**

by

Maida Mahmood

A thesis submitted to the Faculty of the University of Delaware in partial fulfillment of the requirements for the degree of Master in Materials Science and Engineering

Winter 2024

© 2024 Maida Mahmood
All Rights Reserved

**UNDERSTANDING THE IMPACT OF LIGNIN-DERIVABLE NON-
ISOCYANATE POLYURETHANE (NIPU) CHEMISTRY ON
ELECTROSPINNABILITY AND FIBER QUALITY**

by

Maida Mahmood

Approved: _____
LaShanda T. J. Korley, Ph.D.
Professor in charge of thesis on behalf of the Advisory Committee

Approved: _____
Thomas H. Epps, III, Ph.D.
Professor in charge of thesis on behalf of the Advisory Committee

Approved: _____
Joshua Zide, Ph.D.
Chair of the Department of Materials Science and Engineering

Approved: _____
Levi T. Thompson, Ph.D.
Dean of the College of Engineering

Approved: _____
Louis F. Rossi, Ph.D.
Vice Provost for Graduate and Professional Education and
Dean of the Graduate College

ACKNOWLEDGMENTS

I would like to start by thanking the almighty Allah for granting me wisdom, patience, and bonds that I love and cherish. I am forever grateful for the love and support of my parents, Mahmood Ahmad and Tahira Parveen, my sisters Dania Mahmood, Noshaba Mahmood, Mahnoor Mahmood, and my brother-in-law Tahir Waseem. I would also like to extend my heartiest gratitude to Phil Lowe and Paula Lowe for their extraordinary compassion and generosity, and to Sabin, Aidan and Kim for fostering a sense of kinship.

I am deeply thankful to my advisors, Prof. LaShanda T. J. Korley and Prof. Thomas H. Epps, III, for their guidance, expertise, and encouragement throughout the entire research process. They provided invaluable insights and played a crucial role in shaping the direction of this work. I would like to take this opportunity to acknowledge my admiration for Prof. Korley as one of my female role models in STEM. I would also like to thank my committee, Prof. Charles Dhong and Prof. Erik Thostenson, for offering their invaluable perspectives, guidance, and time.

I would like to thank all my brilliant colleagues and mentors from Korley and Epps groups who helped me learn, guided me with patience, and were tremendously generous with their knowledge, particularly Zachary Hinton, Robert O'Dea, Gregory Peterson, Zoé Schyns, Alex Balzer, Jignesh Mahajan, Garrett Bass, and Laura Beckett. I find myself deeply inspired by their brilliance and kindness. I would like to extend a special thanks to my friends at work for their encouragement and support, particularly Daseul Jang, Sara Yang, Yu-Tai Wong, Sampanna Mhatre, and Jamael Ajah. I would

also like to thank my friends outside of work with whom I shared some of the most beautiful memories in my graduate journey: Tasnim Mouri, Sophie Sharafi, Atoofa Zainab, Afia Sarwar, Qurat-ul-ain Bhatti, Umer Sohail, Masooma Sarfraz, and Sarah Dellorco to name a few.

I would not have been able to complete my work without the support of the brilliant UD staff: Dr. Gerald Poirier, Dr. Yong Zhao, Dr. Steve Bai, Kathy Forwood, Dr. Yamy Gonzalez, Dr. F. Scott Stinner, and Dr. Weihua Deng. My work would not be possible without the equipment and support from the Advanced Materials Characterization Lab, Keck Center for Advanced Microscopy & Microanalysis, NMR facility, Center for Plastics Innovation (CPI), and the labs of Dr. Charles Dhong, Dr. Eric M. Furst, and Dr. Michael Mackay.

Lastly, I am deeply grateful for the funding I received from the Higher Education Commission of Pakistan, the US Department of Energy, and the National Science Foundation to complete my research.

TABLE OF CONTENTS

LIST OF TABLES	viii
LIST OF FIGURES	ix
ABSTRACT	xii
Chapter	
1 INTRODUCTION AND MOTIVATION	1
1.1 Introduction	1
1.1.1 Polyurethanes: Consumption, Applications, and Challenges	1
1.1.2 Non-Isocyanate Polyurethane Alternatives	2
1.1.3 Lignocellulosic Biomass as a Sustainable Feedstock for NIPUs ..	4
1.2 Background.....	5
1.2.1 Electrospinning as a Tool for Nanofiber Fabrication	5
1.2.2 Challenges and Limitations of Conventional Electrospinning	6
1.2.3 Literature Review	7
1.2.3.1 Role of Secondary Interactions in Electrospinning	7
1.2.3.2 Bio-based NIPUs for Electrospinning	8
1.3 Key Research Question	9
1.4 Significance of Research	9
REFERENCES	10
2 ELECTROSPINNING OF LIGNIN-DERIVABLE NON-ISOCYANATE POLYURETHANES (NIPU) AND IMPACT OF VARYING NIPU CHEMISTRY ON ELECTROSPINNABILITY AND FIBER MORPHOLOGY	15
2.1 Materials and Methods	15
2.1.1 Materials	15
2.1.2 Synthesis of NIPUs.....	16
2.1.2.1 BGA-NIPU	16
2.1.2.2 BGF-NIPU.....	19
2.1.2.3 BPA-NIPU.....	20
2.1.3 Electrospinning of NIPUs.....	20

2.1.3.1	Selection of Solvent.....	20
2.1.3.1.1	Calculation of NIPU Solubility Parameters Using the van Krevelen Method.....	21
2.1.3.1.2	Important Trends Encountered in Solubility Parameters and Dielectric Constant of Solvents to Promote Electrospinnability of NIPUs	22
2.1.3.2	Selection of Process Parameters	23
2.2	Characterization Techniques:	24
2.2.1	¹ H Nuclear Magnetic Resonance (NMR) Spectroscopy	24
2.2.2	Size Exclusion Chromatography (SEC)	24
2.2.3	Viscosity Measurements.....	25
2.2.4	Conductivity Measurements	25
2.2.5	Scanning Electron Microscopy (SEM).....	25
2.3	Results and Discussion	26
2.3.1	Characterization of Molecular Weight and Dispersity of the NIPUs Used for Electrospinning	26
2.3.2	Analysis of Electrospinning Solution Properties and Fiber Morphology of the NIPUs	28
2.4	Conclusions	31
	REFERENCES	32
3	SUMMARY AND FUTURE WORK	36
3.1	Summary.....	36
3.2	Future Work.....	38
3.2.1	Improving Processibility of Nano-Particle Fillers by Promoting Filler-Matrix Interfacial Adhesion <i>via</i> Hydrogen-Bonding Associations.....	38
3.2.2	Probing the Impact of Hydrogen Bonding on Electrospinning and Fiber Quality of NIPUs <i>via</i> Fourier-transform Infrared (FTIR) Spectroscopy	43
	REFERENCES	46

Appendix

A	SUPPORTING INFORMATION FOR CHAPTER 2	48
B	SUPPORTING INFORMATION FOR CHAPTER 3	59
	B.1 Preparation of Cu-BTC.....	59
	REFERENCES	61

LIST OF TABLES

Table 2.1:	Estimated solubility parameters for BGA-, BGF-, and BPA-NIPUs.....	22
Table 2.2:	Solubility parameters and dielectric constant for various electrospinning solvents.	23
Table 2.3:	Molecular weight data for BPA-, BGA-, and BGF-NIPUs using SEC...	27
Table 2.4:	Electrospinning solution properties and fiber diameter for BPA-, BGA-, and BGF-NIPUs.	29

LIST OF FIGURES

Figure 1.1:	A general synthesis scheme for conventional polyurethanes.	1
Figure 1.2:	A general synthesis scheme for non-isocyanate polyurethanes. The blue circle represents bisguaiacol or bisphenol precursors discussed in more detail in Section 1.1.3 and Figure 1.3.	3
Figure 1.3:	a) Bisguaiacols derived from sustainable lignin feedstocks. b) Bisphenol A derived from petroleum feedstock.	5
Figure 2.1:	Reaction scheme for synthesis of lignin-derivable BGA-NIPU. (a) dimerization of guaiacol to form BGA. (b) Glycidylation of BGA to form BGA diglycidyl ether. (c) Carbonation of diglycidyl ether to form cyclic carbonate. (d) Step-growth polymerization of BGA cyclic carbonate and diaminodecane to form BGA-NIPU.	19
Figure 2.2:	Chemical structures of BGA-, BGF-, and BPA-NIPUs used for electrospinning.	28
Figure 2.3:	SEM micrographs for electrospun fiber mats of BPA-, BGA-, and BGF- NIPUs (10% w/v in HFIP) (a) at high magnification of 10,000 X, and (b) at low magnification of 2000 X (arrows indicating bead formation).	30
Figure 3.1:	(a) Cartoon representing copper ions coordinated with trimesic acid ligands. (b) SEM image of Cu-BTC powder. Particle size estimated: 87 ± 20 nm (average of 50 measurements using ImageJ) (c) PXRD spectrum of Cu-BTC crystals. The grey curve represents simulation done using Materials Studio by Dr. Gregory Peterson from the Epps lab, and the blue curve represents the prepared sample.	40
Figure 3.2:	SEM images for 10% v/v Cu-BTC 15% w/v BPA-NIPU ($M_{n, SEC} = 18.6$ kg/mol; $\bar{D} = 2.8$). The yellow arrows indicate MOF embedding regions, red arrows indicate MOF aggregates, and blue arrows indicate fiber flattening.	42
Figure 3.3:	SEM image (left) alongside EDS elemental maps for carbon (center) and copper (right) for 10% v/v Cu-BTC 15% w/v BPA-NIPU ($M_{n, SEC} = 18.6$ kg/mol; $\bar{D} = 2.8$). The yellow circle indicates the MOF-encapsulation region.	42

Figure 3.4: ATR-FTIR spectra of neat HFIP (red), BPA-NIPU-HFIP solution (black), BPA-NIPU sample after spectral subtraction of HFIP (blue), and BPA-NIPU solid (green) as reference. The highlighted regions indicate urethane stretching (blue, 1700 cm ⁻¹), hydrogen bonding (green, 3000-3500 cm ⁻¹), and reference peak for subtraction (red, 737 cm ⁻¹).....	44
Figure A.1: ¹ H NMR spectrum of Bisguaiacol A (BGA).....	48
Figure A.2: ¹ H NMR spectrum of BGA diglycidyl ether.....	48
Figure A.3: ¹ H NMR spectrum of BGA cyclic carbonate.....	49
Figure A.4: ¹ H NMR spectrum of BGA non-isocyanate polyurethane (NIPU).	49
Figure A.5: ¹ H NMR spectrum of Bisguaiacol F (BGF) NIPU.....	50
Figure A.6: ¹ H NMR spectrum of bisphenol A (BPA) cyclic carbonate.....	50
Figure A.7: ¹ H NMR spectrum of BPA-NIPU.....	51
Figure A.8: Schematic representation of the electrospinning setup (created with BioRender).	51
Figure A.9: Repeat units, molar mass and estimated molar volume of BGA-, BGF-, and BPA-NIPUs.....	52
Figure A.10: Solubility parameter calculations for BPA-NIPU. The values of Van der Waals volume of the structural groups, and the solubility parameter component group contributions (F _{d,i} , F _{p,i} , E _{h,i}) were obtained from the literature. ^{1,2} Molar volume was obtained from the VdW volume as described in the literature. ²	53
Figure A.11: Solubility parameter calculations for BGA-NIPU. The values of Van der Waals volume of the structural groups, and the solubility parameter component group contributions (F _{d,i} , F _{p,i} , E _{h,i}) were obtained from the literature. ^{1,2} Molar volume was obtained from the VdW volume as described in the literature. ²	54
Figure A.12: Solubility parameter calculations for BGF-NIPU. The values of Van der Waals volume of the structural groups, and the solubility parameter component group contributions (F _{d,i} , F _{p,i} , E _{h,i}) were obtained from the literature. ^{1,2} Molar volume was obtained from the VdW volume as described in the literature. ²	55

Figure A.13: Initial electrospinning trials with BPA-NIPU. (a) HFIP produced fibers (diameter = 986 ± 704 nm); DMF-based solution only produced beads. (b) BPA-NIPU spun at ~10% w/v in HFIP produced sub-micron fiber (fiber diameter = 470 ± 203 nm). Process conditions for the trials: flowrate = 0.5 ml/h; tip-collector distance = 15 cm; voltage = 5-6 kV; Needle size = 18 G.....	56
Figure A.14: BPA-, BGA-, and BGF-NIPUs electrospun at ~10% w/v in HFIP at fixed flow rate (0.5 ml/h), tip-to-collector distance (15 cm), and needle diameter (18 G) to determine the operable voltage window.....	56
Figure A.15: SEC chromatograms for BPA-, BGA-, and BGF-NIPUs in DMAc/LiBr (0.5% w/w) using PMMA standards.	57
Figure A.16: Electrospun fiber mats of 10% w/v BPA-NIPU in HFIP. Arrows indicating bead formation. The number of beads was averaged for 5 images at 2000 X magnification, revealing 5 ± 1 beads per $7844 \mu\text{m}^2$...	57
Figure A.17: Electrospun fiber mats of 10% w/v BGA-NIPU in HFIP. Arrows indicating bead formation. The No. of beads was averaged for 5 images at 2000 X magnification, revealing 4 ± 2 beads per $7844 \mu\text{m}^2$...	58
Figure A.18: Electrospun fiber mats of 10% w/v BGF-NIPU in HFIP. Arrows indicating bead formation. No beads were found in this sample as shown in the 2000 X magnification images.	58
Figure B.1: DLS plot of Cu-BTC in DMF (~1 mg/mL). Z Avg. = 149 ± 1 nm; PDI = 0.05 ($PDI = [SDMean]^2$) ³ . Averaged for nine measurements.....	59
Figure B.2: DLS plot of Cu-BTC in HFIP (~1 mg/mL). Z Avg. = 840 ± 54 nm; PDI = 0.21 ($PDI = [SDMean]^2$) ³ . Averaged for nine measurements. ..	60
Figure B.3: Schematic representation of the ATR-FTIR setup used (image created using BioRender). A Teflon gasket was placed around the ATR crystal, and the sample was poured into the gap on top of the crystal. Next, the gap was covered by a glass slide to minimize solvent evaporation during testing.	60

ABSTRACT

Polyurethanes (PUs) are a critical component of the global polymer industry but mainly are derived from fossil fuels and contain hazardous precursors. Non-isocyanate polyurethanes (NIPUs) derived from lignocellulosic biomass, not only provide a safer and sustainable alternative to conventional PUs but also contain functional groups that can alleviate processing challenges and improve electrospinnability. In this work, lignin-derivable bisguaiacol A (BGA)-NIPU (one methoxy group on each aromatic ring with dimethyl bridging substitution) and bisguaiacol F (BGF)-NIPUs (one methoxy group on each aromatic ring without dimethyl bridging substitution) are used to fabricate electrospun fiber mats; and the impact of lignin-derivable NIPU chemistries on electrospinnability and fiber quality is studied. It was found that the presence of methoxy groups in lignin-derivable NIPUs led to a 10-50% increase in viscosity as compared to the bisphenol A (BPA)-NIPU control (no methoxy groups with a dimethyl substitution). Additionally, the absence of dimethyl substitution led to the highest viscosity and completely bead-free fibers in BGF-NIPU in comparison to BPA-NIPU and BGA-NIPU. This work provides an understanding of structure-processing relationships for the electrospinning of lignin-derivable NIPUs. These insights can help inform future studies regarding manufacturing of bio-based NIPU fibers and fiber-composites for different applications.

Chapter 1

INTRODUCTION AND MOTIVATION

1.1 Introduction

1.1.1 Polyurethanes: Consumption, Applications, and Challenges

Polyurethanes (PUs) are a versatile class of polymers, synthesized by step-growth polymerization reaction of polyols and diisocyanates (Figure 1.1).¹ Owing to their multi-faceted chemistry and diverse properties, PUs are among the most widely manufactured polymeric materials worldwide. PUs are the 6th most produced polymer worldwide, with approximately 18 million tons (Mt) of global production in 2016, and an estimated global market value of 56 billion U.S. Dollars (USD).²⁻⁴

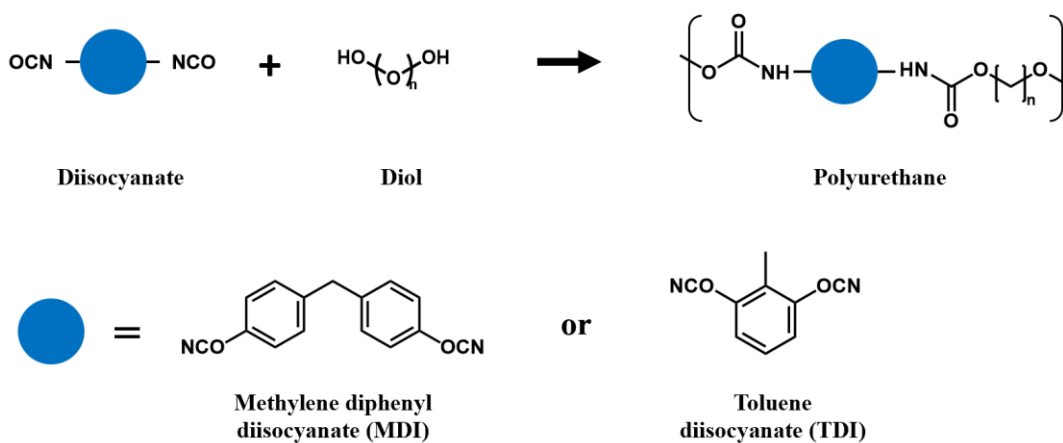


Figure 1.1: A general synthesis scheme for conventional polyurethanes.

Widespread applications of PUs are found in numerous industries such as coatings and adhesives, textiles and fibers, flexible and rigid foams, insulation, construction, sportswear, and packaging.^{2,3,5-7} The availability of tailored precursors for synthesis affords diverse chemical, physical, thermal, and mechanical properties to PUs and allows their use as both thermoset and thermoplastic materials.^{2,5,6} Additionally, the utility of PUs is further advanced by blending them with other polymers and incorporating nanofillers to form composites, thus integrating the benefits of different chemistries.²

PUs are highly desirable materials due to the multiplicity of their chemistry and widespread applications, but their production puts a great toll on the environment. PUs are largely manufactured from non-sustainable petroleum resources and contribute heavily to greenhouse gas (GHG) emissions and environmental pollution.^{4,6,7} The estimated GHG emissions from PU production in the U.S. is approximately 7.8 MMt per annum.⁴ Additionally, the small molecule isocyanate precursors, *i.e.*, toluene diisocyanate (TDI) and methylene diphenyl diisocyanate (MDI) (Figure 1.1), used for PU synthesis are manufactured from highly hazardous phosgene gas.^{1-3,6,8-11} These isocyanates are inherently toxic and can cause severe health problems, including reproductive toxicity, cancer, asthma, and dermatitis.^{1-3,6,8-11} Owing to the sustainability challenges in PU manufacturing and the potential health hazards caused by toxic precursors, there is an urgent demand for sustainably-sourced, non-toxic alternatives with comparable or better properties to replace PUs in the market.

1.1.2 Non-Isocyanate Polyurethane Alternatives

The development of non-isocyanate polyurethane (NIPUs) alternatives has led to polymeric materials which possess the desired PU properties and are more benign in

terms of health hazards.^{1, 2, 11-13} There are various synthetic pathways for NIPUs manufacturing reported in the literature.^{1, 3, 10, 11} Discussed here is the route used to synthesize the NIPUs reported in this study. In this process, the NIPUs are synthesized by the step-growth polymerization reaction of diamines with bis-cyclic carbonates to form hydroxyurethane moieties (Figure 1.2). The resulting polymer in addition to the urethane linkages possesses pendant hydroxyl groups on the backbone. NIPU synthesis avoids the use of toxic isocyanate building blocks (*e.g.*, TDI, MDI), and allows sequestration of carbon dioxide *via* the production of cyclic carbonates, thus making the process more environmentally friendly.^{1, 3, 6, 11-13} Additionally, the presence of pendant hydroxyl groups also can improve the thermomechanical properties, processability, and composite manufacturability of the NIPUs by strengthening secondary interactions.^{6, 11, 13}

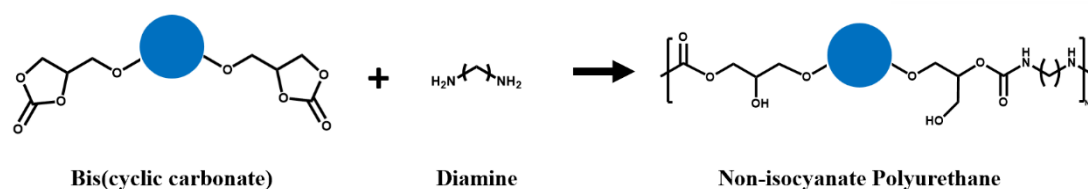


Figure 1.2: A general synthesis scheme for non-isocyanate polyurethanes. The blue circle represents bisguaiacol or bisphenol precursors discussed in more detail in Section 1.1.3 and Figure 1.3.

To further address the sustainability challenges associated with the PU production, several studies have reported the use of bio-based feedstocks for synthesis of NIPU precursors.^{2, 11, 12} The feedstocks used in these reports, although biobased, still are food-competing resources, such as vegetable oils, starches, and sugars.^{2, 11, 12}

The preexisting demand of these feedstocks could potentially hinder the ability for scale-up and industrialization of bio-based NIPUs. Therefore, there is an opportunity to further explore bio-based feedstocks which are readily available, economical, and in need of valorization.

1.1.3 Lignocellulosic Biomass as a Sustainable Feedstock for NIPUs

Lignocellulosic biomass is one of the most abundantly available natural feedstocks, comprised of lignin (15-30%), cellulose (40-60%), and hemicellulose (10-40%).^{9, 14-16} Approximately 50-70 million tons of lignin are extracted from biomass per annum, and roughly 98% of that is used as low-value energy resources.^{9, 14-16} Lignin is the largest source of natural aromatic molecules, and can be depolymerized into a vast library of platform chemicals, which is a tremendously valuable resource in various polymer syntheses, such as NIPUs.^{6, 9, 14}

The aromatic building blocks, such as guaiacols, obtained from lignin depolymerization can be dimerized into bisguaiacols which can help replace toxic chemicals like bisphenol A (BPA) (Figure 1.3). BPA, derived from petroleum resources, is an important platform chemical used in the development of commercial epoxy resin, an essential precursor for NIPU synthesis.^{17, 18} Recognized as a potential endocrine disruptor and reproductive toxin, BPA usage has been shown to lead to various health concerns, such as cardiovascular diseases, diabetes, and cancer.^{8, 15} Lignin-derivable bisguaiacols, on the other hand, have shown weaker binding affinity to the estrogen receptors due to higher steric hindrance introduced by the methoxy substitutions, thereby making bisguaiacols safer and sustainable alternatives of commercial BPA.^{8, 17, 19} Additionally, polymers derived from bisguaiacols have shown comparable thermomechanical properties to those derived from BPA due to the

structural similarities shared by these chemistries. Therefore, bisguaiacols provide a viable platform for the development of sustainable and potentially safer NIPUs.^{8, 17} Moreover, a deeper understanding of NIPU processibility (*e.g.*, fiber and film fabrication, 3D printing) is essential for advancing real-world applications and introducing NIPUs as a practical replacement of PUs in the industry.

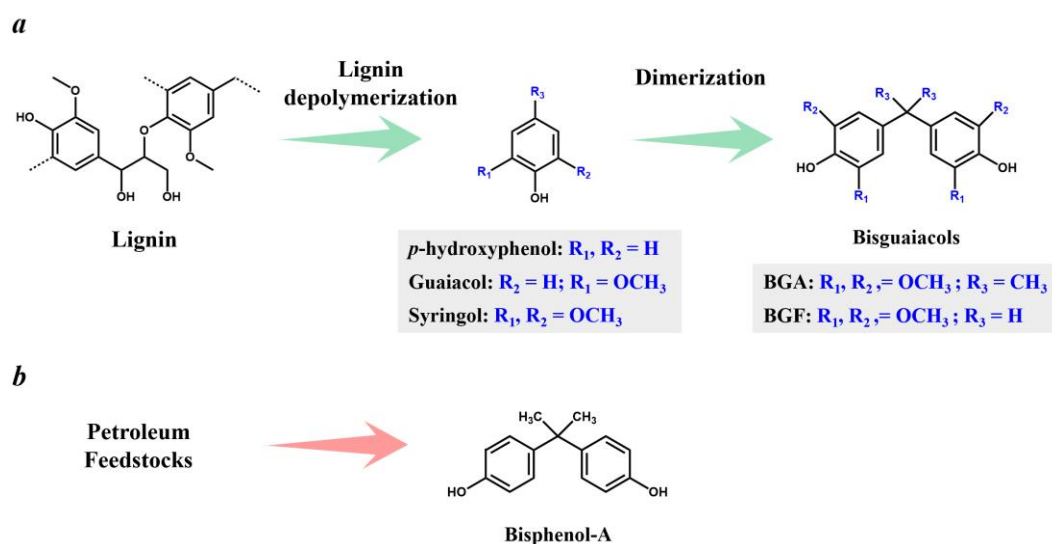


Figure 1.3: a) Bisguaiacols derived from sustainable lignin feedstocks. b) Bisphenol A derived from petroleum feedstock.

1.2 Background

1.2.1 Electrospinning as a Tool for Nanofiber Fabrication

Electrospinning is a technique used to fabricate micro to nanoscale diameter non-woven fibers with high porosity and surface area from polymeric solutions and melts.²⁰⁻²² In typical solvent-based electrospinning, a polymeric solution is charged using an external electric field resulting in the formation of a Taylor cone at the tip of

the syringe nozzle.^{22, 23} A liquid jet emerges from the apex of the Taylor cone and undergoes a series of bending and whipping instabilities, which result in orders-of-magnitude thinning of the jet diameter as well as rapid solvent evaporation and solidification, before it is deposited at a grounded collector.^{21, 23, 24}

Several factors, including polymer properties (*e.g.*, molecular weight, dispersity), solvent quality (*e.g.*, surface tension, dielectric, solubility parameters), process variables (*e.g.*, applied voltage, flowrate, tip-collector distance), and ambient conditions (*e.g.*, humidity, temperature) are essential in successful fabrication of uniform fibers with desired morphology.^{20, 22, 25} The electrospinning process allows tunability of fiber properties and is conducive to filler incorporation, which makes it a favorable fiber manufacturing technique for various applications, such as protective textiles, tissue engineering, drug delivery, air and water purification, stimuli responsive and shape-memory applications, and biomedical sensor technology.^{23, 25}

1.2.2 Challenges and Limitations of Conventional Electrospinning

The electrospinnability of a polymeric solution is indicated by its ability to form bead-free uniform fibers. Bead formation is a result of capillary jet-breakup caused by Rayleigh instabilities.²⁶⁻²⁸ A polymeric solution requires a sufficiently entangled network of polymer chains and long relaxation times to resist the jet-breakup during bending instabilities.²⁶⁻²⁹ As established in prior literature, an increase in polymer molecular weight and/or concentration can add to the number of chain entanglements in a polymeric solution, leading to smooth and uniform electrospun fibers.²⁶⁻³¹ In addition to polymer concentration and molecular weight, certain additives, such as salts and surfactants, also can aid the electrospinnability of a polymer solution by increasing conductivity and electric charge buildup or by

lowering surface tension, respectively.^{29, 32, 33} However, these conventional approaches can lead to various challenges, such as limiting the electrospinnability to high molecular weight polymers and compromising the ability to control fiber diameter and nanostructure due to high polymer concentration. Additionally, the incorporation of additives in the system could lead to complex undesirable interactions with other material components in end applications.

1.2.3 Literature Review

1.2.3.1 Role of Secondary Interactions in Electrospinning

An alternative approach to promote electrospinnability in traditionally non-spinnable polymer solutions, is the use of secondary interactions (*i.e.*, hydrogen bonding, electrostatic interactions) to provide similar constraints as chain entanglements to resist jet-breakup.³⁴ Several reports have been published regarding use of small molecule crosslinkers, supramolecular assemblies, polymer blends, and grafting of hydrogen-bonding functional groups onto polymer chains to promote secondary interactions within polymer solutions, and thereby improve electrospinnability.³⁴⁻⁴⁰ For instance, Hermida-Merino *et al.* reported successful electrospinning of micron size fibers from low molecular weight, self-assembling polyurethanes crafted with hydrogen-bonding end groups.³⁵ Long and co-workers have extensively investigated the impact of supramolecular interactions on solution rheology and electrospinning.^{36, 40, 41} In one example, Long and co-workers reported an increase in viscosity dependence of concentration as well as larger than predicted fiber diameters for poly(methyl methacrylate) with self-complementary hydrogen-bonding motifs compared to the non-associating controls.³⁶ Additionally, Wang *et al.*

reported electrospinning of low molecular weight poly(4-vinylpyridine) with the help of supramolecular small molecule biphenol crosslinkers, providing coordination interactions in the polymer solution.³⁹

1.2.3.2 Bio-based NIPUs for Electrospinning

Provided the effectiveness of secondary interactions in promoting electrospinnability, there is an opportunity to leverage the inherent hydrogen-bonding functionalities of NIPUs to facilitate fabrication of electrospun fibers. Based on our literature review, there is only one prior report of electrospinning of NIPUs. Long *et al.* reported fabrication of free-standing fiber mats from plant-oil-based NIPUs.⁴² In this study, they investigated thermomechanical properties, and moisture uptake of NIPUs fiber mats and addressed their potential for biomedical applications, such as tissue scaffolds and wound dressings. However, it is yet to be understood how the hydrogen-bonding functionality of NIPUs impacts the viscoelastic properties of the solution, and consequently the electrospinnability and fiber quality of the polymers.

In addition to hydroxyl groups, lignin-derivable NIPUs contain methoxy functional groups, which can further promote the hydrogen-bonding capabilities of NIPUs by adding more hydrogen-bonding acceptor sites to the polymer chain. In a previous report by Mhatre *et al.*, it was shown that the presence of methoxy groups in lignin-derivable NIPU thermosets resulted in enhanced toughness and tensile properties by enhancing hydrogen-bonding associations within thermoset networks.⁶ Therefore, there is an opportunity to further investigate the impact of lignin-derivable NIPU chemistries with additional hydrogen-bonding functional groups on electrospinnability and fiber morphology.

1.3 Key Research Question

The aim of this research is to study the effect of methoxy groups and bridging carbon substitution in lignin-derivable NIPUs on electrospinnability and fiber quality. To succeed in this objective, the key question addressed in this thesis is whether the presence of methoxy groups enhances the processibility and fiber quality of lignin-derivable NIPUs by providing more hydrogen-bonding acceptor sites on the polymer backbone and thereby strengthening the secondary interactions within the electrospinning solution.

1.4 Significance of Research

It is anticipated that this study will help to advance the understanding of the impact of lignin-derivable NIPU chemistry on electrospinnability and establish structure-processing relationships. The findings presented in this work will help to expand current subject knowledge of sustainable and potentially non-toxic NIPU nanofibers, which can be useful for various biomedical applications requiring materials for human contact. Therefore, this work will set the stage for future studies in several focused application areas, such as fiber meshes for wound dressing, tissue scaffolds, protective textiles, and sustainable fiber-based composites.

REFERENCES

1. Gomez-Lopez, A.; Elizalde, F.; Calvo, I.; Sardon, H., Trends in non-isocyanate polyurethane (NIPU) development. *Chemical Communications* **2021**, 57 (92), 12254-12265.
2. Carré, C.; Ecochard, Y.; Caillol, S.; Avérous, L., From the Synthesis of Biobased Cyclic Carbonate to Polyhydroxyurethanes: A Promising Route towards Renewable Non-Isocyanate Polyurethanes. *ChemSusChem* **2019**, 12 (15), 3410-3430.
3. Cornille, A.; Auvergne, R.; Figovsky, O.; Boutevin, B.; Caillol, S., A perspective approach to sustainable routes for non-isocyanate polyurethanes. *European Polymer Journal* **2017**, 87, 535-552.
4. Liang, C.; Gracida-Alvarez, U. R.; Gallant, E. T.; Gillis, P. A.; Marques, Y. A.; Abramo, G. P.; Hawkins, T. R.; Dunn, J. B., Material Flows of Polyurethane in the United States. *Environmental Science & Technology* **2021**, 55 (20), 14215-14224.
5. Akindoyo, J. O.; Beg, M. D. H.; Ghazali, S.; Islam, M. R.; Jeyaratnam, N.; Yuvaraj, A. R., Polyurethane types, synthesis and applications – a review. *RSC Advances* **2016**, 6 (115), 114453-114482.
6. Mhatre, S. V.; Mahajan, J. S.; Epps, T. H., III; Korley, L. T. J., Lignin-derivable alternatives to petroleum-derived non-isocyanate polyurethane thermosets with enhanced toughness. *Materials Advances* **2023**, 4 (1), 110-121.
7. Yadav, A.; de Souza, F. M.; Dawsey, T.; Gupta, R. K., Recent Advancements in Flame-Retardant Polyurethane Foams: A Review. *Industrial & Engineering Chemistry Research* **2022**, 61 (41), 15046-15065.
8. Amitrano, A.; Mahajan, J. S.; Korley, L. T. J.; Epps, T. H., III, Estrogenic activity of lignin-derivable alternatives to bisphenol A assessed via molecular docking simulations. *RSC Advances* **2021**, 11 (36), 22149-22158.
9. Bass, G. F.; Epps, T. H., III, Recent developments towards performance-enhancing lignin-based polymers. *Polymer Chemistry* **2021**, 12 (29), 4130-4158.
10. Kathalewar, M. S.; Joshi, P. B.; Sabnis, A. S.; Malshe, V. C., Non-isocyanate polyurethanes: from chemistry to applications. *RSC Advances* **2013**, 3 (13), 4110-4129.

11. Maisonneuve, L.; Lamarzelle, O.; Rix, E.; Grau, E.; Cramail, H., Isocyanate-Free Routes to Polyurethanes and Poly(hydroxy Urethane)s. *Chemical Reviews* **2015**, *115* (22), 12407-12439.
12. Nohra, B.; Candy, L.; Blanco, J.-F.; Guerin, C.; Raoul, Y.; Mouloungui, Z., From Petrochemical Polyurethanes to Biobased Polyhydroxyurethanes. *Macromolecules* **2013**, *46* (10), 3771-3792.
13. Guan, J.; Song, Y.; Lin, Y.; Yin, X.; Zuo, M.; Zhao, Y.; Tao, X.; Zheng, Q., Progress in Study of Non-Isocyanate Polyurethane. *Industrial & Engineering Chemistry Research* **2011**, *50* (11), 6517-6527.
14. O'Dea, R. M.; Willie, J. A.; Epps, T. H., III, 100th Anniversary of Macromolecular Science Viewpoint: Polymers from Lignocellulosic Biomass. Current Challenges and Future Opportunities. *ACS Macro Letters* **2020**, *9* (4), 476-493.
15. Mahajan, J. S.; O'Dea, R. M.; Norris, J. B.; Korley, L. T. J.; Epps, T. H., III, Aromatics from Lignocellulosic Biomass: A Platform for High-Performance Thermosets. *ACS Sustainable Chemistry & Engineering* **2020**, *8* (40), 15072-15096.
16. Gandini, A., The irruption of polymers from renewable resources on the scene of macromolecular science and technology. *Green Chemistry* **2011**, *13* (5), 1061-1083.
17. Nicastro, K. H.; Kloxin, C. J.; Epps, T. H., III, Potential Lignin-Derived Alternatives to Bisphenol A in Diamine-Hardened Epoxy Resins. *ACS Sustainable Chemistry & Engineering* **2018**, *6* (11), 14812-14819.
18. Breitsameter, J. M.; Reinhardt, N.; Feigel, M.; Hinrichsen, O.; Drechsler, K.; Rieger, B., Synthesis of a Sustainable and Bisphenol A-Free Epoxy Resin Based on Sorbic Acid and Characterization of the Cured Thermoset. *Macromolecular Materials and Engineering* **2023**, *308* (9), 2300068.
19. Koelewijn, S.-F.; Ruijten, D.; Trullemans, L.; Renders, T.; Van Puyvelde, P.; Witters, H.; Sels, B. F., Regioselective synthesis, isomerisation, in vitro oestrogenic activity, and copolymerisation of bisguaiacol F (BGF) isomers. *Green Chemistry* **2019**, *21* (24), 6622-6633.
20. Greiner, A.; Wendorff, J. H., Electrospinning: A Fascinating Method for the Preparation of Ultrathin Fibers. *Angewandte Chemie International Edition* **2007**, *46* (30), 5670-5703.

21. Shin, Y. M.; Hohman, M. M.; Brenner, M. P.; Rutledge, G. C., Electrospinning: A whipping fluid jet generates submicron polymer fibers. *Applied Physics Letters* **2001**, *78* (8), 1149-1151.
22. Salas, C., 4 - Solution electrospinning of nanofibers. In *Electrospun Nanofibers*, Afshari, M., Ed. Woodhead Publishing: 2017; pp 73-108.
23. Xue, J.; Wu, T.; Dai, Y.; Xia, Y., Electrospinning and Electrospun Nanofibers: Methods, Materials, and Applications. *Chemical Reviews* **2019**, *119* (8), 5298-5415.
24. Hohman, M. M.; Shin, M.; Rutledge, G.; Brenner, M. P., Electrospinning and electrically forced jets. I. Stability theory. *Physics of Fluids* **2001**, *13* (8), 2201-2220.
25. Haider, A.; Haider, S.; Kang, I.-K., A comprehensive review summarizing the effect of electrospinning parameters and potential applications of nanofibers in biomedical and biotechnology. *Arabian Journal of Chemistry* **2018**, *11* (8), 1165-1188.
26. Shenoy, S. L.; Bates, W. D.; Frisch, H. L.; Wnek, G. E., Role of chain entanglements on fiber formation during electrospinning of polymer solutions: good solvent, non-specific polymer-polymer interaction limit. *Polymer* **2005**, *46* (10), 3372-3384.
27. Ewaldz, E.; Randrup, J.; Brettmann, B., Solvent Effects on the Elasticity of Electrospinnable Polymer Solutions. *ACS Polymers Au* **2022**, *2* (2), 108-117.
28. McKee, M. G.; Wilkes, G. L.; Colby, R. H.; Long, T. E., Correlations of Solution Rheology with Electrospun Fiber Formation of Linear and Branched Polyesters. *Macromolecules* **2004**, *37* (5), 1760-1767.
29. Fong, H.; Chun, I.; Reneker, D. H., Beaded nanofibers formed during electrospinning. *Polymer* **1999**, *40* (16), 4585-4592.
30. Gupta, P.; Elkins, C.; Long, T. E.; Wilkes, G. L., Electrospinning of linear homopolymers of poly(methyl methacrylate): exploring relationships between fiber formation, viscosity, molecular weight and concentration in a good solvent. *Polymer* **2005**, *46* (13), 4799-4810.
31. Wojasiński, M.; Ciach, T., Shear and elongational rheometry for determination of spinnability window of polymer solutions in solution blow spinning. *Journal of Applied Polymer Science* **2022**, *139* (36), e52851.

32. Tong, L.; Hongxia, W.; Huimin, W.; Xungai, W., The charge effect of cationic surfactants on the elimination of fibre beads in the electrospinning of polystyrene. *Nanotechnology* **2004**, *15* (9), 1375.
33. Nartetamrongsutt, K.; Chase, G. G., The influence of salt and solvent concentrations on electrospun polyvinylpyrrolidone fiber diameters and bead formation. *Polymer* **2013**, *54* (8), 2166-2173.
34. Ewaldz, E.; Brettmann, B., Molecular Interactions in Electrospinning: From Polymer Mixtures to Supramolecular Assemblies. *ACS Applied Polymer Materials* **2019**, *1* (3), 298-308.
35. Hermida-Merino, D.; Belal, M.; Greenland, B. W.; Woodward, P.; Slark, A. T.; Davis, F. J.; Mitchell, G. R.; Hamley, I. W.; Hayes, W., Electrospun supramolecular polymer fibres. *European Polymer Journal* **2012**, *48* (7), 1249-1255.
36. McKee, M. G.; Elkins, C. L.; Long, T. E., Influence of self-complementary hydrogen bonding on solution rheology/electrospinning relationships. *Polymer* **2004**, *45* (26), 8705-8715.
37. Meng, X.; Du, Y.; Liu, Y.; Coughlin, E. B.; Perry, S. L.; Schiffman, J. D., Electrospinning Fibers from Oligomeric Complex Coacervates: No Chain Entanglements Needed. *Macromolecules* **2021**, *54* (11), 5033-5042.
38. Uyar, T.; Havelund, R.; Nur, Y.; Balan, A.; Hacaloglu, J.; Toppare, L.; Besenbacher, F.; Kingshott, P., Cyclodextrin functionalized poly(methyl methacrylate) (PMMA) electrospun nanofibers for organic vapors waste treatment. *Journal of Membrane Science* **2010**, *365*, 409-417.
39. Wang, X.; Pellerin, C.; Bazuin, C. G., Enhancing the Electrospinnability of Low Molecular Weight Polymers Using Small Effective Cross-Linkers. *Macromolecules* **2016**, *49* (3), 891-899.
40. Yamauchi, K.; Lizotte, J. R.; Long, T. E., Thermoreversible Poly(alkyl acrylates) Consisting of Self-Complementary Multiple Hydrogen Bonding. *Macromolecules* **2003**, *36* (4), 1083-1088.
41. McKee, M. G.; Layman, J. M.; Cashion, M. P.; Long, T. E., Phospholipid Nonwoven Electrospun Membranes. *Science* **2006**, *311* (5759), 353-355.

42. Aduba Jr, D. C.; Zhang, K.; Kanitkar, A.; Serrine, J. M.; Verbridge, S. S.; Long, T. E., Electrospinning of plant oil-based, non-isocyanate polyurethanes for biomedical applications. *Journal of Applied Polymer Science* **2018**, *135* (29), 46464.

Chapter 2

ELECTROSPINNING OF LIGNIN-DERIVABLE NON-ISOCYANATE POLYURETHANES (NIPU) AND IMPACT OF VARYING NIPU CHEMISTRY ON ELECTROSPINNABILITY AND FIBER MORPHOLOGY

2.1 Materials and Methods

2.1.1 Materials

Guaiacol (99+%, Thermo Scientific), thioglycolic acid ($\geq 98\%$, Sigma-Aldrich), hydrochloric acid (HCl, 37% w/w, Thermo Scientific), epichlorohydrin ($\geq 99\%$, Fulka Analytical), tetrabutylammonium bromide (TBAB, $\geq 99\%$, Acros Organic), sodium hydroxide (NaOH, 98.7%, Fisher Chemicals), 1,10-diaminodecane (97%, Thermo Scientific), lithium chloride (LiCl, $\geq 99\%$, Sigma-Aldrich), acetone (Optima grade, 99.5%, Fisher Chemical), dichloromethane (DCM, 99.9%, HPLC grade, Fisher Chemical), dimethyl sulfoxide (DMSO, 99.7%, Acros Organic), deuterated dimethyl sulfoxide (DMSO- d_6 , 99.5+ atom% D, Thermo Scientific), tetrahydrofuran (THF, containing 0.025% butylated hydroxytoluene as inhibitor, Fisher Chemical), Bisphenol A diglycidyl ether (BADGE, 340.41 g/mol, Sigma-Aldrich), hexafluoroisopropanol (HFIP, $\geq 99\%$, MP Biomedicals), dimethyl formamide (DMF, 99.8%, ACS grade, Fisher Chemical), dimethyl acetamide (DMAc, HPLC grade, Fisher Chemical), lithium bromide (LiBr, $\geq 99\%$, Sigma-Aldrich).

2.1.2 Synthesis of NIPUs

2.1.2.1 BGA-NIPU

Lignin-derivable NIPUs were prepared using a multistep process, including the synthesis of bisguaiacol-based monomers, bisguaiacol diglycidyl ethers, cyclic carbonates, and NIPUs (Figure 2.1).

BGA monomer was synthesized following the procedure developed by Mhatre *et al.* (Figure 2.1a).¹ Guaiacol (40 g, 0.32 mol) and acetone dried using magnesium sulfate (3.4 mL, 0.046 mol) were added to a 250-mL, single-neck, round-bottom flask. Next, concentrated HCl (4 mL, 15 w/w% of guaiacol) was added to the reaction flask, followed by thioglycolic acid (0.16 mL). The reaction mixture was purged with Ar for 10 min and later stirred, using a magnetic stir bar (500 rpm), at 100 °C for 24 h. Afterwards, the reaction mixture was allowed to cool to 25 °C and dissolved in 15 mL of DCM. The reaction mixture was then washed with aqueous sodium bicarbonate (3x) using a separatory funnel. The organic phase was then washed with deionized (DI) water (3x) followed by washing with brine solution (3x). Next, the product was purified by flash column chromatography using Biotage Selekt automated flash system with Biotage Sfar Silica columns (60 µm particle size, 100 Å, 100 g silica gel), and for elution employing a step gradient of ethyl acetate (25% v/v) and hexanes (75% v/v). Rotary evaporation was then used to remove the majority of solvents from the product followed by drying at 50 °C under vacuum (Fisherbrand Isotemp Model 281A vacuum oven, Fisherbrand MaximaDry diaphragm vacuum pump). Finally, the molecular structure of BGA was confirmed using proton nuclear magnetic resonance (¹H NMR) spectroscopy (A.1)

Bisguaiacol A diglycidyl ether (BGADGE) was synthesized following the procedure developed by Nicastro *et al.* (Figure 2.1b).² BGA (0.02 mol), epichlorohydrin (0.2 mol), and TBAB (0.002 mol) were added to a 50-mL, single-neck, round bottom flask and stirred, using a magnetic stir bar (500 rpm), and sparged with Ar at 20 °C for 30 min. The mixture was then heated at 50 °C in an oil bath for 2 h. The reaction mixture was immediately cooled in an ice bath at 0 °C for 10 min and then transferred to a water bath at 25 °C. Aqueous NaOH (0.08 mol) was then added dropwise to the reaction mixture followed by stirring for 16 h at 25 °C and 500 rpm. After completion of the reaction, the mixture was dissolved in DCM (10 mL) and washed in a separatory funnel with DI water (until the pH of aqueous phase was neutral), and then with brine solution (3x). Next, the organic phase was purified by flash column chromatography using Biotage Selekt automated flash system with Biotage Sfär Silica columns (60 µm particle size, 100 Å, 100 g silica gel), and for elution employing a step gradient of ethyl acetate (60% v/v) and hexanes (40% v/v). Rotary evaporation was then used to remove majority of solvents from the product followed by drying of the concentrated product at 50 °C under vacuum (Fisherbrand Isotemp Model 281A vacuum oven, Fisherbrand MaximaDry diaphragm vacuum pump). Finally, the molecular structure of BGADGE was confirmed using ¹H NMR spectroscopy (A.2).

Bisguaiacol A cyclic carbonate (BGA-CC) was synthesized following the procedure developed by Mhatre *et al.* (Figure 2.1b).¹ BGADGE (3 g, 0.0075 mol), and TBAB (0.036 g, 1.2% w/w) were added to a cylindrical Teflon liner together with a magnetic stir bar and then sealed into a 25-mL Parr reactor. The mixture was then purged with CO₂ (3x), pressurized with 30 bars of CO₂ at 130 °C, and stirred for 24 h

at 200 rpm. After completion, the reaction mixture was allowed to cool to 25 °C followed by depressurization of the reactor. The product was then dissolved in acetone (2 mL) and precipitated in DI water (2x) followed by drying of the precipitates at 65 °C under vacuum (Fisherbrand Isotemp Model 281A vacuum oven, Fisherbrand MaximaDry diaphragm vacuum pump). Finally, the molecular structure of BGA-CC was confirmed using ¹H NMR spectroscopy (A.3).

BGA-NIPU was synthesized following the procedure developed by Mahajan *et al* (Figure 2.1b).³ BGA-CC (1 g, 0.002 mol), diaminodecane (0.34 g, 0.002 mol), and LiCl (8 mg, 0.2 mmol) were added to a 25-mL, single-neck, round bottom flask with a magnetic stir bar. DMSO (2 mL, 1 mL/1 mmol of BGA-CC) was then added to the reaction flask, the mixture was purged with Ar for 30 min at 100 °C and 500 rpm, and the reaction was continued at 100 °C for 24 h. After completion, the reaction mixture was dissolved in THF (3 mL) and precipitated in DI water (3x). The precipitated product was dried at 90 °C for 48 h under vacuum (Fisherbrand Isotemp Model 281A vacuum oven, Fisherbrand MaximaDry diaphragm vacuum pump). Finally, the molecular structure of BGA-NIPU was confirmed using ¹H NMR spectroscopy (A.4).

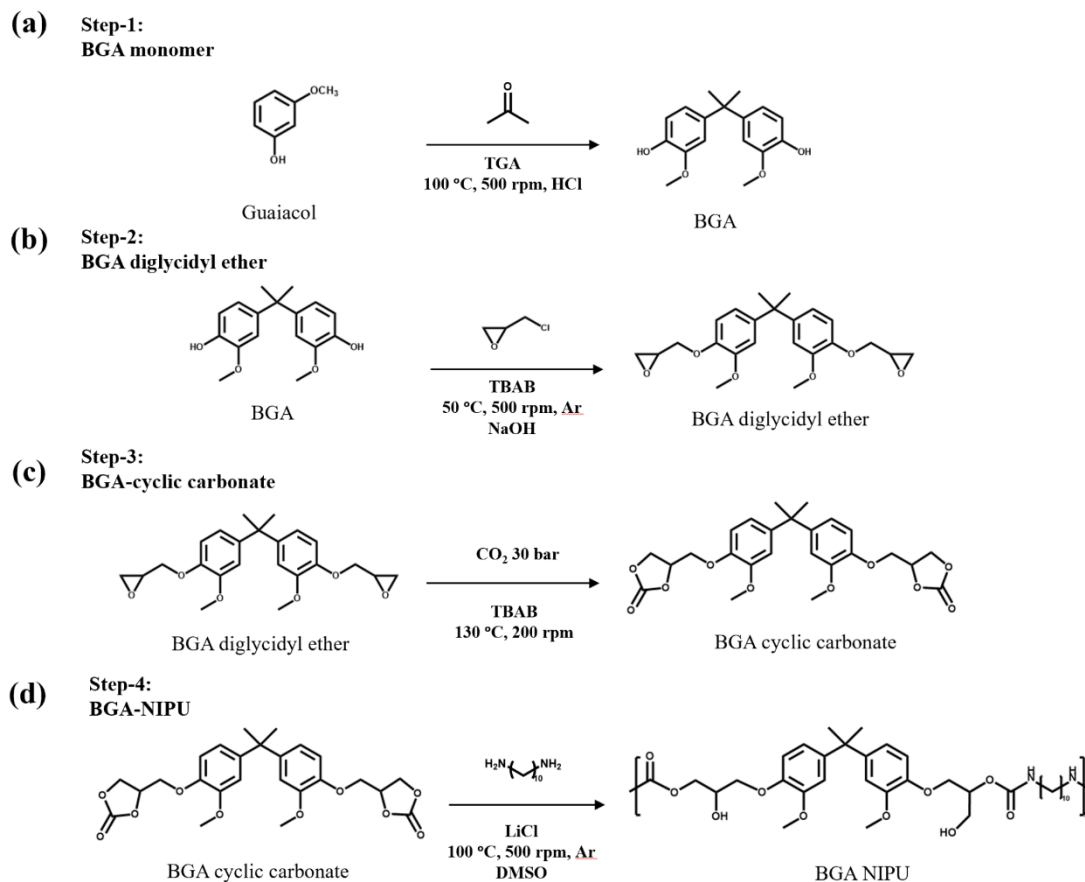


Figure 2.1: Reaction scheme for synthesis of lignin-derivable BGA-NIPU. (a) dimerization of guaiacol to form BGA. (b) Glycidylation of BGA to form BGA diglycidyl ether. (c) Carbonation of diglycidyl ether to form cyclic carbonate. (d) Step-growth polymerization of BGA cyclic carbonate and diaminodecane to form BGA-NIPU.

2.1.2.2 BGF-NIPU

The procedure for BGF-monomer synthesis is described in Mhatre et.al.¹ For this study, bisguaiacol F cyclic carbonate (BGF-CC) was synthesized and donated by Jignesh Mahajan from the Korley and Epps labs. The diglycidyl ether and cyclic carbonate were synthesized following the procedures described earlier for BGADGE, BGA-CC in Section 2.1.2.1. BGF-CC was then used to prepare BGF-NIPU following

the procedure described in Section 2.1.2.1 for BGA-NIPU synthesis. The molecular structure of BGA-NIPU was confirmed using ^1H NMR (Figure A.5).

2.1.2.3 BPA-NIPU

Bisphenol A cyclic carbonate (BPA-CC) was synthesized from commercially available BADGE following the same procedure as discussed in Section 2.1.2.1 for bisguaiacol cyclic carbonate. BPA-CC was then converted into BPA-NIPU using the same procedure as discussed in Section 2.1.2.1 for lignin-derivable NIPUs. The characterization of molecular structures was done using ^1H NMR (BPA-CC in Figure A.6; BPA-NIPU in Figure A.7).

2.1.3 Electrospinning of NIPUs

All NIPUs were electrospun using an electrospinning setup built in-house (Figure A.8). The setup consisted of a programmable syringe pump (Braintree Scientific BS-8000) to dispense the solution at a set flowrate, a reusable blunt tip needle connected with disposable plastic syringe to carry the polymeric solution, a power supply (Genvolt 7xx30 series, 0–20 kV output) to provide tunable voltage, and a grounded flat plate collector covered with aluminum foil for fiber deposition. The entire electrospinner was enclosed in an acrylic cage equipped with safety interlock switch to cut off the voltage supply when opened and limit exposure to solvent vapors.

2.1.3.1 Selection of Solvent

Solvent properties, such as the solubility parameters and dielectric constants, were used to guide the selection of optimal solvent for electrospinning of NIPUs.

2.1.3.1.1 Calculation of NIPU Solubility Parameters Using the van Krevelen Method

Solubility parameters (δ) can be used to predict the solubility of a given solute in a solvent by relating a molecular motif's cohesive energies to their molar volumes. Solubility is maximized in systems in which the solvent and solute have a similar δ .⁴ The group contribution method by van Krevelen, accounting for polar, dispersive, and hydrogen-bonding components (δ_p , δ_d , δ_h , respectively) of the solubility parameter, was used to estimate the solubility parameters of NIPUs *via* their molecular structure as shown in Eq. 2.1 - 2.4.⁴ The estimated solubility parameters provided additional insight into the individual contribution of polar, dispersive, and hydrogen-bonding forces towards solubility of NIPUs in various electrospinning solvents.⁴

$$\delta_d = \frac{\sum F_{d,i}}{V} \quad (2.1)$$

$$\delta_p = \frac{\sqrt{\sum F_{p,i}^2}}{V} \quad (2.2)$$

$$\delta_h = \frac{\sqrt{\sum E_{h,i}}}{V} \quad (2.3)$$

$$\delta_t = \sqrt{\delta_d^2 + \delta_p^2 + \delta_h^2} \quad (2.4)$$

Here, F_d , F_p , and E_h represent dispersive, polar, and hydrogen-bonding energy contributions, respectively; V is the molar volume of the polymer repeat unit; and δ_t is the total solubility parameter. The molecular structure, molar mass, and molar volume of repeat units of the NIPUs are presented in Figure A.9. Calculations for solubility parameters for BPA-, BGA-, and BGF-NIPUs are provided in Figures A.10 – A.12, respectively, and the estimated solubility parameters are summarized in Table 2.1.

Table 2.1: Estimated solubility parameters for BGA-, BGF-, and BPA-NIPUs.

Polymer matrix	Solubility Parameters			
	δ_d (MPa) ^{0.5}	δ_p (MPa) ^{0.5}	δ_h (MPa) ^{0.5}	δ_t (MPa) ^{0.5}
BGA-NIPU	19.2	2.5	11.8	22.7
BGF-NIPU	19.5	2.7	12.2	23.1
BPA-NIPU	17.6	2.3	11.4	21.1

2.1.3.1.2 Important Trends Encountered in Solubility Parameters and Dielectric Constant of Solvents to Promote Electrospinnability of NIPUs

In initial electrospinning trials, common electrospinning solvents were chosen according to prior literature (Table 2.2).⁵⁻⁸ The values of solubility parameters and dielectric constant for the selected solvents were obtained from literature.⁹⁻¹¹ The distance between solvent and NIPU coordinates on the solubility sphere (D_{s-p}) was calculated by incorporating solubility parameters for NIPUs and solvents provided in Tables 2.1 and 2.2, respectively, into Eq 2.5, to estimate polymer-solvent compatibility (Table 2.2).^{12, 13} As established in previous studies, smaller D_{s-p} values indicate better compatibility between the solvent and the polymer.^{12, 13} According to calculated D_{s-p} values, HFIP displayed the highest compatibility with the studied NIPU matrices (Table 2.2). Additionally, HFIP displayed the highest hydrogen-bonding parameter, lowest polarity, and low dielectric constant, which potentially could enhance hydrogen-bonding interactions between the NIPU chains and the solvent.^{6, 14-16} In the initial electrospinning trials, HFIP produced uniform BPA-NIPU fibers, whereas DMF only produced beads. The THF-based solution was not spinnable

due to needle clogging, potentially caused by high solvent volatility. Therefore, HFIP was selected as the electrospinning solvent of all NIPU samples. It is noted here that HFIP is considered a toxic solvent, and future work may involve exploration of greener solvents with similar solubility parameters, such as dimethyl carbonate, as a safer alternative for electrospinning.¹⁷ Details of the initial trials with the selected solvents and BPA-NIPU are provided in supporting information (Figure A.13a)

$$D_{s-p} = \sqrt{4(\delta_{dS} - \delta_{dP})^2 + (\delta_{pS} - \delta_{pP})^2 + (\delta_{hS} - \delta_{hP})^2} \quad (2.5)$$

Here, $\delta_{(d,p,h)S}$, and $\delta_{(d,p,h)P}$ represent the dispersive, polar, and hydrogen-bonding parameters for the solvent and polymer, respectively.

Table 2.2: Solubility parameters and dielectric constant for various electrospinning solvents.

Solvent	Solubility Parameters ^{9, 10} (MPa ^{0.5})				Solubility coordinates D_{s-p}			Dielectric constant ¹¹
	δ_d	δ_p	δ_h	δ_t	BPA-NIPU	BGF-NIPU	BGA-NIPU	
HFIP	17.2	4.3	14.7	23	3.9	5.5	5.3	16.7
DMF	17.4	13.7	11.3	24.9	11.4	11.8	11.8	36.7
THF	16.8	5.7	8	19.5	5.1	7.5	6.9	7.6

2.1.3.2 Selection of Process Parameters

As mentioned earlier in Section 1.2.1, several electrospinning parameters can impact the spinnability and fiber morphology of polymeric systems. A polymer concentration of 10% w/v was selected, as it produced submicron fibers compared to 15% w/v which produced micron sized fibers in initial solvent trials, (Figure A.13a and A.13b). Next, applied voltage was optimized for all NIPU samples while keeping tip-collector distance, needle gauge, flowrate, and humidity constant at 15 cm, 18 G,

0.5 mL/h, and $50 \pm 5\%$, respectively. An operable range of applied voltage was established for BGA-NIPU (6–8 kV), BGF-NIPU (6–8 kV) and BPA-NIPUs (5–6 kV) by changing the voltage during electrospinning and identifying a window in which the voltage is neither insufficient to form a jet, nor too high to cause multiple jetting (Figure A.14). Finally, 6 kV was selected as the optimum voltage for electrospinning of all NIPUs.

All NIPU solutions were prepared by dissolving chosen NIPUs in HFIP (10% w/v) under constant stirring for 16 h at 500 rpm and 25 °C. All electrospun fiber mats were dried at 50 °C under vacuum (Fisherbrand Isotemp Model 281A vacuum oven; Fisherbrand MaximaDry diaphragm vacuum pump) for 48 h prior to characterization.

2.2 Characterization Techniques:

2.2.1 ¹H Nuclear Magnetic Resonance (NMR) Spectroscopy

The molecular structure of the synthesized monomers, diglycidyl ethers, cyclic carbonates and NIPUs were confirmed by ¹H-NMR spectra using an AVIII 600 MHz Bruker (5 mm SMART probe) (in DMSO-d₆) at room temperature. The recorded spectra were analyzed using MestReNova.

2.2.2 Size Exclusion Chromatography (SEC)

SEC was performed to measure number average and weight average molecular weights (M_n and M_w , respectively), and dispersity (\mathcal{D}) of the NIPUs using a TOSOH Bioscience EcoSEC Elite system with TSKgel columns (one SuperAW-L guard column, one SuperAW2500 column, and two Super AWM-H columns) and refractive index (RI) detector. DMAc stabilized with 0.5 wt% LiBr was used as the mobile phase. 80 μ L of polymer dissolved in mobile phase was eluted for 45 min at 0.4 mL/min and 50 °C. Samples were calibrated against six poly(methyl methacrylate)

(PMMA) standards (675.5 kg/mol; 260.9 kg/mol; 72 kg/mol; 30.7 kg/mol; 4.7 kg/mol; 1.7 kg/mol). All SEC samples were prepared by dissolving 1 mg/mL of polymer in the mobile phase for 48 h and filtering the solution twice through a 0.1 μm PTFE filter.

2.2.3 Viscosity Measurements

Viscosity measurements were conducted using a BYK Gardner CAP 2000+ Viscometer. CAP spindle No.1 was used for all measurements, and calibration was performed *via* CANNON CAP1L (89 mPa-s) standard. All viscosity measurements were performed at 25 °C and averaged for a total of six measurements for BGA-, BGF-, and BPA-NIPUs. The samples were prepared by taking an aliquot (100 μL per measurement) from the NIPU electrospinning solutions, prepared as described in Section 2.1.3.2.

2.2.4 Conductivity Measurements

Electrical conductivity measurements were conducted using an InLab 731-ISM sensor connected to Mettler Toledo Conductivity Meter at 25 °C for BGA-, BGF-, and BPA-NIPUs. The conductivity readings were allowed to stabilize (~15 s) before the measurements were recorded. The samples were prepared by taking an aliquot (5 mL per measurement) from the NIPU electrospinning solutions, prepared as described in Section 2.1.3.2.

2.2.5 Scanning Electron Microscopy (SEM)

Fiber morphology was examined *via* SEM using an Auriga 60 CrossBeam (FE-SEM/FIB) at an accelerating voltage of 3 kV. The electrospun fiber mats were cut out along with the aluminum foil and sputter coated with a layer of Au/Pd before

imaging. Fiber diameter was measured using image processing software (ImageJ) and averaged for 100 individual fiber diameter measurements for BGA-, BGF-, and BPA-NIPUs.

2.3 Results and Discussion

2.3.1 Characterization of Molecular Weight and Dispersity of the NIPUs Used for Electrospinning

To understand the impact of lignin derivable NIPU chemistry on electrospinning, samples were chosen with varying degrees of hydrogen-bonding capability. Two lignin-derivable NIPUs, BGA-NIPU (one methoxy group on each aromatic ring with a dimethyl bridging substitution) and BGF-NIPU (one methoxy group on each aromatic ring without a dimethyl bridging substitution), and a petroleum-based control BPA-NIPU (without any methoxy groups on the aromatic rings and with a dimethyl bridging substitution) were selected (Figure 2.2). It was anticipated that the presence of methoxy groups would increase secondary interactions and consequently the viscosity in the polymer solution, improving solution electrospinnability. The number and weight average molecular weights and dispersity of the prepared NIPUs were determined using SEC. The molecular weight data are presented in Table 2.3 and the SEC chromatographs are shown in Figure A.15.

Table 2.3: Molecular weight data for BPA-, BGA-, and BGF-NIPUs using SEC.

Polymer	$M_{n, SEC}$ (kg/mol)	$M_{w, SEC}$ (kg/mol)	\bar{D}
BPA-NIPU	19.3	81.6	4.2
BGA-NIPU	18.5	78.0	4.2
BGF-NIPU	21.0	75.6	3.5

The molecular weight and molecular weight distribution of a polymer are known to have significant impact on the viscoelastic properties and consequently electrospinnability of a polymer solution.¹⁸⁻²³ Moreover, the weight-average molecular weight (M_w), which shows larger dependence on the presence of high molecular weight chains, is of high importance, especially in polymers with high molecular weight distribution such as those used in this study.^{18, 24} It has been shown that the presence of high molecular weight species in the polymer solution can improve both processability and fiber quality of polymer solutions.^{18, 22, 24} Therefore, for a direct comparison of samples, the M_w for all NIPUs samples was kept approximately equivalent to minimize the overall impact of molecular weight on electrospinning outcomes and thereby isolate the impact of polymer structure on electrospinnability.

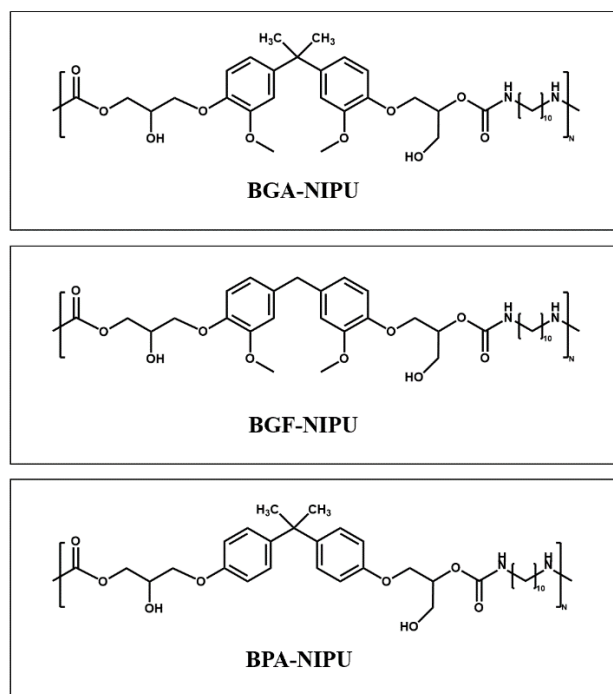


Figure 2.2: Chemical structures of BGA-, BGF-, and BPA-NIPUs used for electrospinning.

2.3.2 Analysis of Electrospinning Solution Properties and Fiber Morphology of the NIPUs

At a fixed polymer concentration of 10% w/v, BGA-NIPU samples showed roughly 10% higher viscosity than the BPA-NIPU control (Table 2.4), which was attributed to potentially higher hydrogen bonding between the polymer and HFIP solvent. An increase in viscosity can be favorable for electrospinning, and high viscosity solutions have shown to be more resistant towards jet breakup and bead formation.¹⁹⁻²³ However, it was suspected that the bridging carbon substitutions could weaken hydrogen bonding of the methoxy groups on the aromatic rings by increasing the steric hindrance and decreasing the surface area available for formation of hydrogen bonds.^{25, 26} Therefore, BGF-NIPU, which has the same number of methoxy

groups as BGA-NIPU and no bridging substitution, was electrospun to promote hydrogen bonding in the NIPU solution.

It was found that BGF-NIPU had a viscosity value of 51% higher than the BPA-NIPU control (Table 2.4), confirming that reducing steric hindrance appears to improve hydrogen bonding and increase resulting viscosity. All NIPUs produced continuous fibers as shown in (Figure 2.3a) with BPA- and BGA-NIPU fibers containing small number of beads, and BGF-NIPU generating completely bead-free fibers (Figure 2.3b and A.16-18). These defect-free, BGF-NIPU electrospun fibers may be due to its higher solution viscosity stemming from a potential increase in polymer-solvent interactions.

Table 2.4: Electrospinning solution properties and fiber diameter for BPA-, BGA-, and BGF-NIPUs.

Polymer	Polymer conc. (% w/v)	Solvent	Viscosity η_0 (mPa-s)	Conductivity σ ($\mu\text{S}/\text{cm}$)	Fiber diameter (nm)
BPA-NIPU	10	HFIP	47 ± 2	29.3	273 ± 98
BGA-NIPU	10	HFIP	52 ± 3	--	334 ± 107
BGF-NIPU	10	HFIP	71 ± 6	35.4	246 ± 98

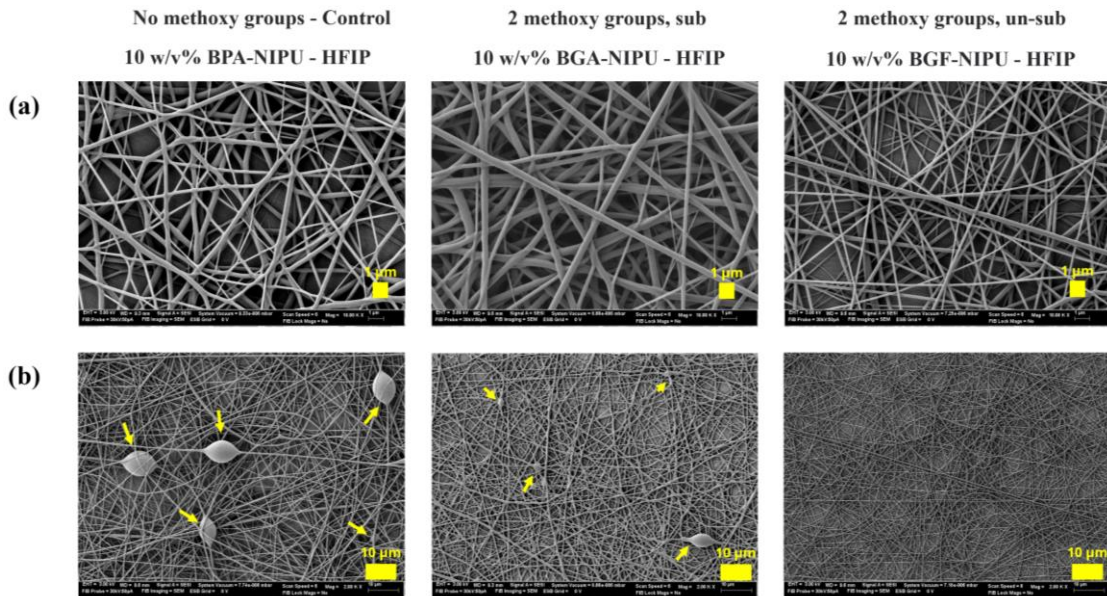


Figure 2.3: SEM micrographs for electrospun fiber mats of BPA-, BGA-, and BGF-NIPUs (10% w/v in HFIP) (a) at high magnification of 10,000 X, and (b) at low magnification of 2000 X (arrows indicating bead formation).

The fiber diameter for NIPUs remained unchanged across all samples. However, BGF-NIPU did not follow the previously established trends of larger fiber diameter with an increase in solution viscosity.²⁷⁻²⁹ According to prior literature, in addition to viscosity, properties, such as solution conductivity, also can significantly influence fiber diameter.²⁷⁻³⁰ Higher conductivity allows greater charge buildup, leading to increased stretching and elongation of the liquid jet and resulting in thinning of fiber diameter.²⁷⁻²⁹ Therefore, the conductivity of the BGF-NIPU solution was compared with the BPA-NIPU control and was found to be higher (Table 2.4). A higher solution conductivity could contribute to the decrease in fiber diameter in BGF-NIPU fiber mats. In addition, it is noted that higher weight-average molecular weight of the NIPUs may play a dominate role in this analysis, in comparison to the effects of

the solution properties (*i.e.*, viscosity, conductivity) and potentially leading to consistent fiber diameter across all NIPU samples.

Furthermore, the variability of fiber diameter is a pivotal challenge of the electrospinning process, which can be mitigated by optimization of process parameters and the use of additives.^{20, 31, 32} It was found that maintaining a constant voltage led to a noticeable change in the standard deviation of fiber diameter for NIPUs, decreasing from 200-700 nm in the initial trial stage to 100 nm upon maintaining a constant voltage. Subsequent studies could enhance the fiber diameter control by exploring the use of additives, such as salts and surfactants, as discussed in previous studies.^{31, 32} Finally, the fiber diameter was below 500 nm for all samples, which can be beneficial from an application standpoint due to the high surface area of nanoscale fiber mats.

2.4 Conclusions

In this chapter, the effects of polymer-solvent interactions, and their influence on solution viscosity, were highlighted as initial estimates of the electrospinnability of NIPU-based materials. Systems with more hydrogen-bonding sites and less steric hindrance, such as lignin-derivable BGF-NIPU, yielded uniform, bead-less fibers. In contrast, systems with increased steric hindrance and fewer numbers of solvent-polymer interactions, such as the petroleum-based BPA-NIPU control, exhibited lower viscosity leading to reduced homogeneity and formation of beads in electrospun fibers. Ultimately, these fibers can be utilized in a vast variety of applications, specifically those requiring sustainably sourced nanofibers with potentially non-toxic precursors, such as wound dressings and tissue scaffolds.

REFERENCES

1. Mhatre, S. V.; Mahajan, J. S.; Epps, T. H., III; Korley, L. T. J., Lignin-derivable alternatives to petroleum-derived non-isocyanate polyurethane thermosets with enhanced toughness. *Materials Advances* **2023**, *4* (1), 110-121.
2. Nicastro, K. H.; Kloxin, C. J.; Epps, T. H., III, Potential Lignin-Derived Alternatives to Bisphenol A in Diamine-Hardened Epoxy Resins. *ACS Sustainable Chemistry & Engineering* **2018**, *6* (11), 14812-14819.
3. J. S. Mahajan, Z. R. H., E. Nombera-Bueno, T. H. Epps, III, L.T. J. Korley, Lignin-derivable, thermoplastic, non-isocyanate polyurethanes with increased hydrogen-bonding content and toughness as potential alternatives to petroleum-derived analogues. In *Materials Advances*, in preparation.
4. Van Krevelen, D. W.; Te Nijenhuis, K., Chapter 7 - Cohesive Properties and Solubility. In *Properties of Polymers (Fourth Edition)*, Van Krevelen, D. W.; Te Nijenhuis, K., Eds. Elsevier: Amsterdam, 2009; pp 189-227.
5. Aduba Jr, D. C.; Zhang, K.; Kanitkar, A.; Serrine, J. M.; Verbridge, S. S.; Long, T. E., Electrospinning of plant oil-based, non-isocyanate polyurethanes for biomedical applications. *Journal of Applied Polymer Science* **2018**, *135* (29), 46464.
6. McKee, M. G.; Elkins, C. L.; Long, T. E., Influence of self-complementary hydrogen bonding on solution rheology/electrospinning relationships. *Polymer* **2004**, *45* (26), 8705-8715.
7. Peterson, G. W.; Lu, A. X.; Epps, T. H., III, Tuning the Morphology and Activity of Electrospun Polystyrene/UiO-66-NH₂ Metal–Organic Framework Composites to Enhance Chemical Warfare Agent Removal. *ACS Applied Materials & Interfaces* **2017**, *9* (37), 32248-32254.
8. Wang, X.; Pellerin, C.; Bazuin, C. G., Enhancing the Electrospinnability of Low Molecular Weight Polymers Using Small Effective Cross-Linkers. *Macromolecules* **2016**, *49* (3), 891-899.
9. Barton, A. F. M., *CRC Handbook of Solubility Parameters and Other Cohesion Parameters (Second Edition)*. Routledge: New York, 1991.
10. Hansen, C. M., *Hansen Solubility Parameters : A User's Handbook (Second Edition)*. CRC Press: Boca Raton, 2007.

11. Smallwood, I. M., *Solvent Recovery Handbook (Second Edition)*. CRC Press: New York, 2002.
12. Kurban, Z.; Lovell, A.; Bennington, S. M.; Jenkins, D. W. K.; Ryan, K. R.; Jones, M. O.; Skipper, N. T.; David, W. I. F., A Solution Selection Model for Coaxial Electrospinning and Its Application to Nanostructured Hydrogen Storage Materials. *The Journal of Physical Chemistry C* **2010**, *114* (49), 21201-21213.
13. T.Senthil, D.; Anandhan, S., Effect of Solvents on the Solution Electrospinning of Poly(styrene-co-acrylonitrile). *KGK rubberpoint* **2017**.
14. Cheuk, K. K. L.; Lam, J. W. Y.; Chen, J.; Lai, L. M.; Tang, B. Z., Amino Acid-Containing Polyacetylenes: Synthesis, Hydrogen Bonding, Chirality Transcription, and Chain Helicity of Amphiphilic Poly(phenylacetylene)s Carrying l-Leucine Pendants. *Macromolecules* **2003**, *36* (16), 5947-5959.
15. Boileau, S.; Bouteiller, L.; Lauprêtre, F.; Lortie, F., Soluble supramolecular polymers based on urea compounds. *New Journal of Chemistry* **2000**, *24* (11), 845-848.
16. Colomer, I.; Chamberlain, A. E. R.; Haughey, M. B.; Donohoe, T. J., Hexafluoroisopropanol as a highly versatile solvent. *Nature Reviews Chemistry* **2017**, *1* (11), 0088.
17. Oldal, D. G.; Topuz, F.; Holtzl, T.; Szekely, G., Green Electrospinning of Biodegradable Cellulose Acetate Nanofibrous Membranes with Tunable Porosity. *ACS Sustainable Chemistry & Engineering* **2023**, *11* (3), 994-1005.
18. Palangetic, L.; Reddy, N. K.; Srinivasan, S.; Cohen, R. E.; McKinley, G. H.; Clasen, C., Dispersity and spinnability: Why highly polydisperse polymer solutions are desirable for electrospinning. *Polymer* **2014**, *55* (19), 4920-4931.
19. Ewaldz, E.; Randrup, J.; Brettmann, B., Solvent Effects on the Elasticity of Electrospinnable Polymer Solutions. *ACS Polymers Au* **2022**, *2* (2), 108-117.
20. Fong, H.; Chun, I.; Reneker, D. H., Beaded nanofibers formed during electrospinning. *Polymer* **1999**, *40* (16), 4585-4592.
21. Gupta, P.; Elkins, C.; Long, T. E.; Wilkes, G. L., Electrospinning of linear homopolymers of poly(methyl methacrylate): exploring relationships between fiber formation, viscosity, molecular weight and concentration in a good solvent. *Polymer* **2005**, *46* (13), 4799-4810.

22. McKee, M. G.; Wilkes, G. L.; Colby, R. H.; Long, T. E., Correlations of Solution Rheology with Electrospun Fiber Formation of Linear and Branched Polyesters. *Macromolecules* **2004**, *37* (5), 1760-1767.
23. Shenoy, S. L.; Bates, W. D.; Frisch, H. L.; Wnek, G. E., Role of chain entanglements on fiber formation during electrospinning of polymer solutions: good solvent, non-specific polymer–polymer interaction limit. *Polymer* **2005**, *46* (10), 3372-3384.
24. Srinivasan, S.; Chhatre, S. S.; Mabry, J. M.; Cohen, R. E.; McKinley, G. H., Solution spraying of poly(methyl methacrylate) blends to fabricate microtextured, superoleophobic surfaces. *Polymer* **2011**, *52* (14), 3209-3218.
25. Nowok, A.; Dulski, M.; Grelska, J.; Szeremeta, A. Z.; Jurkiewicz, K.; Grzybowska, K.; Musiał, M.; Pawlus, S., Phenyl Ring: A Steric Hindrance or a Source of Different Hydrogen Bonding Patterns in Self-Organizing Systems? *The Journal of Physical Chemistry Letters* **2021**, *12* (8), 2142-2147.
26. Pérez-Casas, S.; Moreno-Esparza, R.; Costas, M.; Patterson, D., Effect of steric hindrance and π electrons on alcohol self-association. *Journal of the Chemical Society, Faraday Transactions* **1991**, *87* (11), 1745-1750.
27. Xue, J.; Wu, T.; Dai, Y.; Xia, Y., Electrospinning and Electrospun Nanofibers: Methods, Materials, and Applications. *Chemical Reviews* **2019**, *119* (8), 5298-5415.
28. Haider, A.; Haider, S.; Kang, I.-K., A comprehensive review summarizing the effect of electrospinning parameters and potential applications of nanofibers in biomedical and biotechnology. *Arabian Journal of Chemistry* **2018**, *11* (8), 1165-1188.
29. Greiner, A.; Wendorff, J. H., Electrospinning: A Fascinating Method for the Preparation of Ultrathin Fibers. *Angewandte Chemie International Edition* **2007**, *46* (30), 5670-5703.
30. Ding, X.; Li, Y.; Si, Y.; Yin, X.; Yu, J.; Ding, B., Electrospun polyvinylidene fluoride/SiO₂ nanofibrous membranes with enhanced electret property for efficient air filtration. *Composites Communications* **2019**, *13*, 57-62.
31. Deitzel, J.; Kleinmeyer, J.; Harris, D. E. A.; Beck Tan, N., The Effect of Processing Variables on the Morphology of Electrospun Nanofibers and Textiles. *Polymer* **2001**, *42*, 261-272.

32. Lin, K.; Chua, K.-N.; Christopherson, G. T.; Lim, S.; Mao, H.-Q., Reducing electrospun nanofiber diameter and variability using cationic amphiphiles. *Polymer* **2007**, *48* (21), 6384-6394.
33. Van Krevelen, D. W.; Te Nijenhuis, K., Chapter 4 - Volumetric Properties. In *Properties of polymers (Fourth Edition)*, Van Krevelen, D. W.; Te Nijenhuis, K., Eds. Elsevier: Amsterdam, 2009; pp 71-108.

Chapter 3

SUMMARY AND FUTURE WORK

3.1 Summary

Developing safer and sustainably sourced thermoplastics is a key step towards achieving a circular plastics economy. In this thesis, the chemistry of lignin-derivable non-isocyanate polyurethanes (NIPUs), which are emerging biobased alternatives to conventional petroleum-based polyurethanes (PUs), was leveraged to facilitate electrospinning of bead-free uniform nanofibers.

NIPUs derived from lignin-derivable building blocks possess backbones featuring chemical motifs, such as methoxy groups and dimethyl bridging substitutions, which result in varying hydrogen-bonding capabilities and can be engineered to promote the manufacturability of NIPUs. The presence of methoxy groups has previously been shown to enhance the mechanical properties of NIPU thermosets by increasing hydrogen-bonding associations across the network structure.¹ Moreover, the presence of dimethyl bridging substitutions can impact the hydrogen bonding of methoxy groups by contributing to the steric hindrance in the polymer backbone. Hydrogen-bonding associations have been shown to improve electrospinnability of polymeric solutions by providing similar constraints as chain entanglements and resisting jet break-up in the instability zones during electrospinning.²⁻⁵ Building on previous studies, the hydrogen-bonding chemical motifs of biobased NIPUs were manipulated to promote electrospinnability in this research. Specifically, the impact of hydrogen-bonding capabilities, related to NIPU chemistry, on electrospinnability and fiber morphology was further studied. By tuning

fiber morphology through the choice of functional groups on the polymer backbone of lignin-derivable NIPUs, uniform fibers can be achieved.

To probe the effects of backbone chemistry, two lignin-derivable NIPUs, BGA-NIPU (one methoxy group on each aromatic ring with a dimethyl bridging substitution), and BGF-NIPU (one methoxy group on each aromatic rings without a dimethyl bridging substitution) were used for electrospinning. Additionally, BPA-NIPU (without any methoxy groups on the aromatic rings and with a dimethyl bridging substitution) was selected as a petroleum-based control. The molecular weight and molecular weight distribution of all NIPUs were kept approximately equivalent to minimize the impact of molecular weight on electrospinning. Moreover, all electrospinning parameters (*i.e.*, flowrate, voltage, tip-collector distance, polymer concentration, solvent quality, and humidity) were kept consistent across all NIPU samples to isolate the impact of chemical structure on electrospinnability. Solubility parameter calculations were used to select an optimal solvent to maximize electrospinning success. From initial approximations, HFIP displayed the favorable D_{s-p} values, hydrogen-bonding parameter, and dielectric constant (Table 2.2), and was selected as the electrospinning solvent for all NIPUs.

Lignin-derivable NIPUs exhibited 10-50% higher viscosity than the BPA-NIPU control (*i.e.*, $\eta_0 = 47 \pm 2$ mPa-s), attributed to increased hydrogen-bonding interactions between the polymer and solvent. Investigating lignin-derivable BGA-NIPU and BGF-NIPU, it emerged that the introduction of dimethyl bridging substitution in BGA-NIPU ($\eta_0 = 52 \pm 3$ mPa-s) resulted in a viscosity reduction compared to BGF-NIPU. The decrease in viscosity was ascribed to an increase in steric hinderance from the presence of methyl groups on the bridging carbon,

potentially compromising the hydrogen-bonding associations of methoxy groups in the polymer solution. In contrast, BGF-NIPU exhibited the highest viscosity among all tested samples (*i.e.*, $\eta_0 = 71 \pm 6$ mPa-s), and consequently was the sole sample generating bead-free fibers. The fiber diameter of BGF-NIPU did not show the expected increase with viscosity, which could be caused by high solution conductivity in BGF-NIPU ($\sigma = 35.4$ $\mu\text{S/cm}$) compared to the BPA-NIPU control ($\sigma = 29.3$ $\mu\text{S/cm}$) and an overall high molecular weight of the NIPU samples.

Finally, the NIPU fibers fabricated in this study can be a promising choice for applications, such as wound dressings, tissue scaffolds, and protective clothing due to the safer and sustainable resources used in their manufacturing. Additionally, the finding presented in this work can be beneficial for expanding current knowledge of sustainable NIPU fibers and establishing structure-processing relationships.

3.2 Future Work

3.2.1 Improving Processibility of Nano-Particle Fillers by Promoting Filler-Matrix Interfacial Adhesion *via* Hydrogen-Bonding Associations

In Chapter 2, it was shown that all NIPUs can be electrospun into nanofibers, and the lignin-derivable NIPUs displayed better solution properties and processability due to the presence of additional hydrogen-bonding associations due to the presence of methoxy groups. The utility of NIPU fibers can be advanced further by the incorporation of fillers, for which the hydrogen-bonding capabilities of NIPUs can be beneficial for promoting filler-matrix interfacial interactions and can lead to improved mechanical performance, and processability in the composites.⁶⁻⁹ To test this concept, Cu-BTC metal organic framework (MOF), which shares structural similarities with

NIPUs and possesses hydrogen-bonding functional groups, was selected as the filler for NIPUs.

MOFs are a class of porous materials with highly crystalline 3D structures, formed by coordination of metal ions and organic ligands.¹⁰ MOFs, in their composite form, are utilized in various applications, such as gas capture and storage, purification, and drug delivery *etc.*¹⁰⁻¹² One of the challenges associated with MOF processing is their aggregation due to high surface charges, especially at high MOF loading (*i.e.*, approximately 50% v/v), leading to compromised microstructure, decreased surface area, and interfacial defects within the composites.^{6, 9-13} NIPUs can potentially form hydrogen-bonding interactions with unsaturated organic MOF ligands, and thereby allow polymeric stabilization to mitigate aggregation, and matrix incompatibility issues. Moreover, lignin derivable NIPUs, with additional hydrogen-bonding sites, can potentially extend the limit of MOF loading to a higher particle concentration.

To explore this idea, Cu-BTC MOF was incorporated into BPA-NIPU to fabricate electrospun composite fiber mats. The structure of Cu-BTC MOF consists of copper ions and dicarboxylic acid ligands (Figure 3.1 (a)). It was anticipated that the hydroxyl groups on the BPA-NIPU backbone will form hydrogen-bonding associations with the unsaturated dicarboxylic acid ligands, leading to encapsulation of the MOF by the NIPU, and consequently preventing MOF aggregation. Cu-BTC nanocrystals were prepared using the procedure described in Wang *et al.*; details of the synthesis conditions are provided in Section B.1.¹⁴ MOF particle size was determined by dynamic light scattering (DLS) (Malver Zetasizer Pro) (Figure B.1) and SEM (Figure 3.1 (b)), and the crystalline structure was confirmed using powder X-ray

diffraction (PXRD) (Bruker D8 XRD, scanned using Cu K α radiations at 40 kV and 40 mA, scan rate of 5° min⁻¹ in a 2-theta range of (4–50)°) (Figure 3.1 (c)).

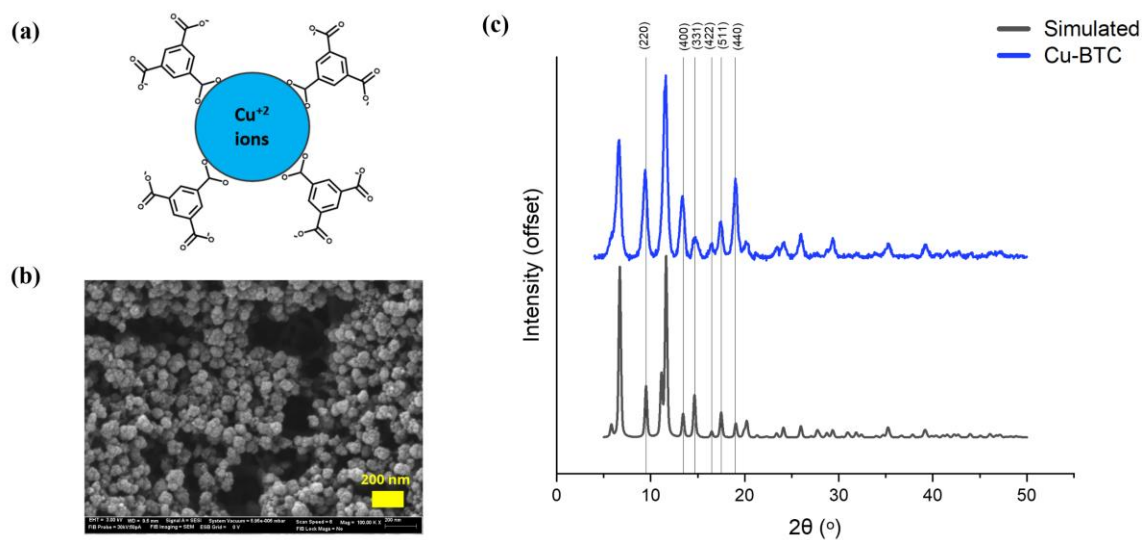


Figure 3.1: (a) Cartoon representing copper ions coordinated with trimesic acid ligands. (b) SEM image of Cu-BTC powder. Particle size estimated: 87 ± 20 nm (average of 50 measurements using ImageJ) (c) PXRD spectrum of Cu-BTC crystals. The grey curve represents simulation done using Materials Studio by Dr. Gregory Peterson from the Epps lab, and the blue curve represents the prepared sample.

The particle size of Cu-BTC crystals was approximately 100–150 nm, according to the DLS measurement of Cu-BTC dispersed in DMF (Figure B.1), and the estimation from the SEM images (Figure 3.1 (b)). However, the particle size increased to 840 ± 54 nm when dispersed in HFIP (Figure B.2), indicating aggregation of Cu-BTC in HFIP. Therefore, the 15% w/v NIPU concentration, which produced 986 ± 704 nm diameter fibers (Figure A.13 (a)), was selected for electrospinning to prevent MOF from bulging out of the fibers in case of successful encapsulation. To

prepare the electrospinning solution, 10% v/v of Cu-BTC was dispersed in HFIP *via* sonication, and 15% w/v BPA-NIPU was gradually added and dissolved into the MOF-HFIP dispersion forming a MOF-ink, which has been shown to aid the dispersion of MOF in the polymer matrix.^{15, 16} Electrospinning was done using previously established processing conditions for BPA-NIPU in Section 2.1.3.2 and Figure A.13 (a).

According to these preliminary findings, the Cu-BTC/BPA-NIPU solution was electrospinnable and produced bead-free fibers of diameter 1072 ± 1050 nm with MOF particles embedded inside (Figure 3.2). The SEM images showed promising morphological features, such as encapsulation of MOF inside the fibers (Figure 3.2, yellow arrows), which has been reported as a sign of filler-matrix compatibility and can be attributed to hydrogen-bonding interaction between the MOF and polymer. The encapsulation of MOF was further confirmed by elemental copper mapping using energy dispersive X-ray spectroscopy (EDS) (Figure 3.3), showing copper clusters inside the fiber. However, the neat NIPU as well as composite NIPU fibers showed significantly large standard deviation in the diameter. The fiber diameter variability in neat NIPU fibers was previously addressed in section 2.3.2, whereas in composite fibers further optimization of process variable is needed. It is also noted that the presence of MOF aggregates (Figure 3.2, red arrows), and an anticipated increase in the solution viscosity upon MOF incorporation, also can contribute towards non-uniformity in fiber morphology (*i.e.*, diameter variability and fiber flattening; Figure 3.2, blue arrows).

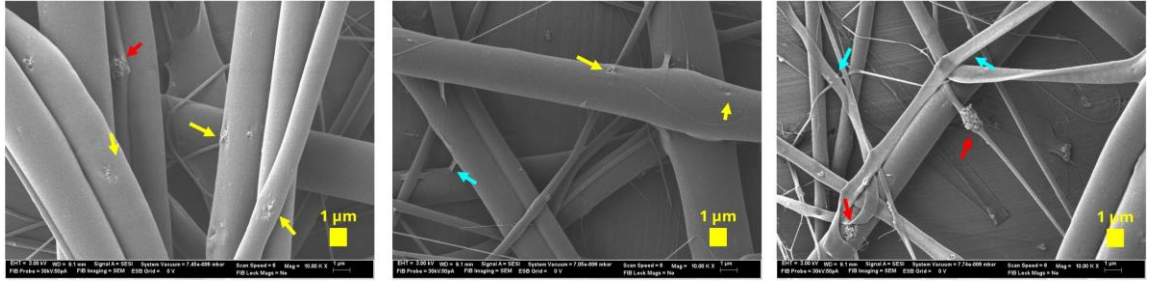


Figure 3.2: SEM images for 10% v/v Cu-BTC 15% w/v BPA-NIPU ($M_n, SEC = 18.6$ kg/mol; $\bar{D} = 2.8$). The yellow arrows indicate MOF embedding regions, red arrows indicate MOF aggregates, and blue arrows indicate fiber flattening.

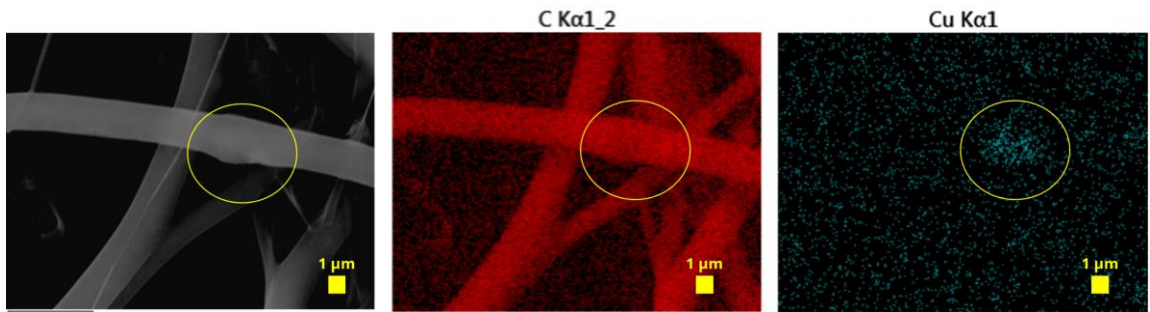


Figure 3.3: SEM image (left) alongside EDS elemental maps for carbon (center) and copper (right) for 10% v/v Cu-BTC 15% w/v BPA-NIPU ($M_n, SEC = 18.6$ kg/mol; $\bar{D} = 2.8$). The yellow circle indicates the MOF-encapsulation region.

To address the challenges in fiber morphology, it is proposed that the future studies investigate the impact of process variables on the electrospinning of particle-filled systems. Additionally, further understanding of MOF-solvent interactions, which can be achieved by a systematic study of MOF-solvent compatibility, is needed to identify and mitigate the cause of MOF aggregation. The quantification of solution viscosity of MOF-NIPU solutions can also help in further optimization of fiber quality of the composites. Moreover, the fabrication and characterization of MOF-NIPU

composites of lignin-derivable systems needs to be conducted. It is anticipated that the lignin-derivable systems will promote favorable MOF-polymer interactions, due to additional hydrogen-bonding sites, and facilitate better dispersion of MOF in the polymer matrix.

3.2.2 Probing the Impact of Hydrogen Bonding on Electrospinning and Fiber Quality of NIPUs via Fourier-transform Infrared (FTIR) Spectroscopy

FTIR spectroscopy serves as an invaluable tool for qualitatively analyzing hydrogen-bonding interactions. In the context of electrospinning of NIPUs, solution FTIR spectroscopy can be vital in understanding the intricate relationship between hydrogen bonding and the electrospinnability, substantiating the claims regarding the diverse hydrogen-bonding capabilities inherent in NIPU structures. As discussed in chapter 2, the presence of methoxy moieties afford lignin-derivable NIPUs additional hydrogen-bonding acceptor sites. Furthermore, the NIPU backbone features multiple hydrogen bond donor (-NH, -OH) and acceptor (O-, -C=O, -O-CH₃) groups. It has been demonstrated that deconvoluting the hydrogen-bonding regions (*i.e.*, 3000–3500 cm⁻¹) can offer insight into the bonded and free hydrogen-bonding sites, which can be a useful strategy for elucidating the varying hydrogen-bonding capabilities of the NIPUs.^{17, 18}

Solution ATR-FTIR was performed to probe secondary interactions in electrospinning solutions using a Thermo Nicolet NEXUS 470 FTIR spectrometer coupled with a Smart Orbit Diamond ATR accessory. The spectra presented in this study were an average of 128 scans recorded with a resolution of 4 cm⁻¹ in the wavelength range of 400–4000 cm⁻¹. A 10% w/v BPA-NIPU/HFIP solution sample, prepared as described in Section 2.1.3.2, was dropped onto the ATR crystal covered

by a Teflon gasket and glass slide to avoid solvent evaporation during testing (Figure B.3). Spectral subtraction was performed, using subtraction tool in OMNIC™ software package, to remove the spectral contribution of HFIP from the NIPU solution. A subtraction factor (SF) of 1.23 was selected following the disappearance of the reference peak at 737 cm^{-1} , present solely in the HFIP spectrum (Figure 3.4).

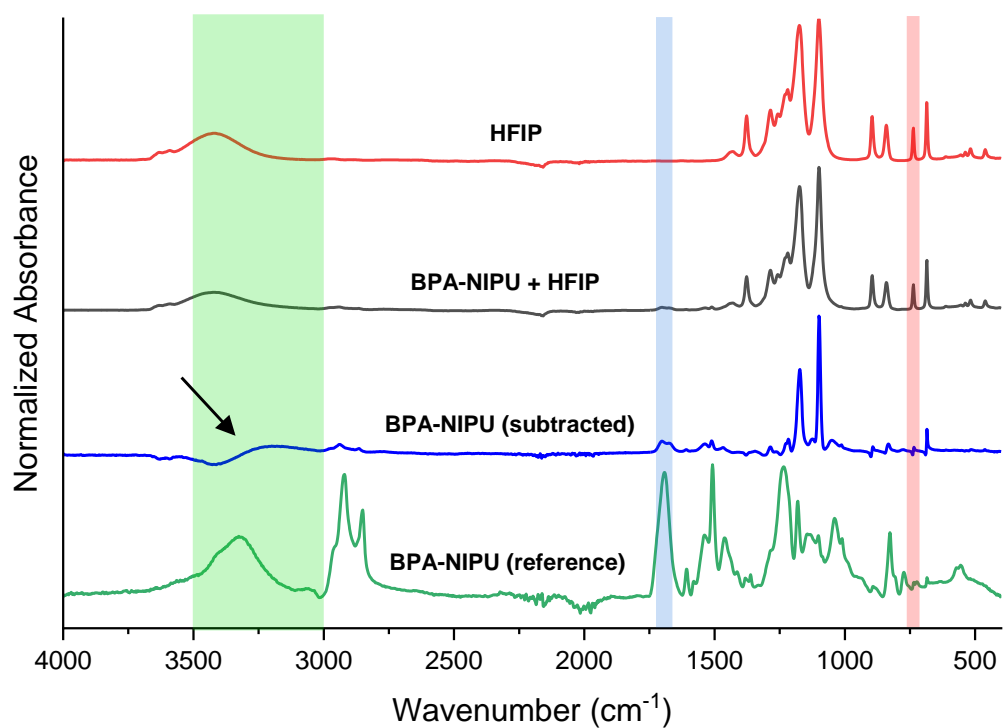


Figure 3.4: ATR-FTIR spectra of neat HFIP (red), BPA-NIPU-HFIP solution (black), BPA-NIPU sample after spectral subtraction of HFIP (blue), and BPA-NIPU solid (green) as reference. The highlighted regions indicate urethane stretching (blue, 1700 cm^{-1}), hydrogen bonding (green, $3000\text{--}3500\text{ cm}^{-1}$), and reference peak for subtraction (red, 737 cm^{-1}).

FTIR spectra collected for 10% w/v BPA-NIPU solution (grey curve), neat HFIP (red curve), and BPA-NIPU solid (green curve) as a reference are shown in Figure 3.4. HFIP is a hydrogen-bonding solvent, and an overlap of IR signals was seen in the hydrogen-bonding region ($3000\text{--}3500\text{ cm}^{-1}$) in both the spectra of neat HFIP and BPA-NIPU solid. In the subtracted spectrum of BPA-NIPU (blue curve), the characteristic urethane stretching band (1700 cm^{-1}) was evident. However, the desired hydrogen-bonding region posed challenges for deconvolution and separation from the spectral contribution of HFIP. Furthermore, the subtracted spectrum exhibited weak signal contributions of BPA-NIPU in comparison to the BPA-NIPU solid, making it difficult to distinguish between the signal and noise. It is anticipated that the low molar concentration of NIPUs in the electrospinning solution (*i.e.*, $\sim 0.02\%$ mol/mol) could result in poor signal to noise ratio and potentially intensify the contribution of contaminants, such as moisture, thereby making the sample less fitting for a qualitative FTIR analysis. Therefore, it is proposed that the future studies explore the use of sufficiently high molar concentration for NIPU solution samples, as well as consider using transmission IR mode to enhance the quality of the subtracted spectrum.

REFERENCES

1. Mhatre, S. V.; Mahajan, J. S.; Epps, T. H., III; Korley, L. T. J., Lignin-derivable alternatives to petroleum-derived non-isocyanate polyurethane thermosets with enhanced toughness. *Materials Advances* **2023**, *4* (1), 110-121.
2. Ewaldz, E.; Brettmann, B., Molecular Interactions in Electrospinning: From Polymer Mixtures to Supramolecular Assemblies. *ACS Applied Polymer Materials* **2019**, *1* (3), 298-308.
3. Hermida-Merino, D.; Belal, M.; Greenland, B. W.; Woodward, P.; Slark, A. T.; Davis, F. J.; Mitchell, G. R.; Hamley, I. W.; Hayes, W., Electrospun supramolecular polymer fibres. *European Polymer Journal* **2012**, *48* (7), 1249-1255.
4. McKee, M. G.; Elkins, C. L.; Long, T. E., Influence of self-complementary hydrogen bonding on solution rheology/electrospinning relationships. *Polymer* **2004**, *45* (26), 8705-8715.
5. Wang, X.; Pellerin, C.; Bazuin, C. G., Enhancing the Electrospinnability of Low Molecular Weight Polymers Using Small Effective Cross-Linkers. *Macromolecules* **2016**, *49* (3), 891-899.
6. Mahdi, E. M.; Tan, J.-C., Mixed-matrix membranes of zeolitic imidazolate framework (ZIF-8)/Matrimid nanocomposite: Thermo-mechanical stability and viscoelasticity underpinning membrane separation performance. *Journal of Membrane Science* **2016**, *498*, 276-290.
7. Mahdi, E. M.; Tan, J.-C., Dynamic molecular interactions between polyurethane and ZIF-8 in a polymer-MOF nanocomposite: Microstructural, thermo-mechanical and viscoelastic effects. *Polymer* **2016**, *97*, 31-43.
8. Fu, S.-Y.; Feng, X.-Q.; Lauke, B.; Mai, Y.-W., Effects of particle size, particle/matrix interface adhesion and particle loading on mechanical properties of particulate-polymer composites. *Composites Part B: Engineering* **2008**, *39* (6), 933-961.
9. Peterson, G. W.; Au, K.; Tovar, T. M.; Epps, T. H., III, Multivariate CuBTC Metal-Organic Framework with Enhanced Selectivity, Stability, Compatibility, and Processability. *Chemistry of Materials* **2019**, *31* (20), 8459-8465.

10. Denny, M. S.; Moreton, J. C.; Benz, L.; Cohen, S. M., Metal–organic frameworks for membrane-based separations. *Nature Reviews Materials* **2016**, *1* (12), 16078.
11. Benzaqui, M.; Semino, R.; Menguy, N.; Carn, F.; Kundu, T.; Guigner, J.-M.; McKeown, N. B.; Msayib, K. J.; Carta, M.; Malpass-Evans, R.; Le Guillouzer, C.; Clet, G.; Ramsahye, N. A.; Serre, C.; Maurin, G.; Steunou, N., Toward an Understanding of the Microstructure and Interfacial Properties of PIMs/ZIF-8 Mixed Matrix Membranes. *ACS Applied Materials & Interfaces* **2016**, *8* (40), 27311-27321.
12. Peterson, G. W.; Lee, D. T.; Barton, H. F.; Epps, T. H., III; Parsons, G. N., Fibre-based composites from the integration of metal–organic frameworks and polymers. *Nature Reviews Materials* **2021**, *6* (7), 605-621.
13. Peterson, G. W.; Lu, A. X.; Epps, T. H., III, Tuning the Morphology and Activity of Electrospun Polystyrene/UiO-66-NH₂ Metal–Organic Framework Composites to Enhance Chemical Warfare Agent Removal. *ACS Applied Materials & Interfaces* **2017**, *9* (37), 32248-32254.
14. Wang, X.-G.; Cheng, Q.; Yu, Y.; Zhang, X.-Z., Controlled Nucleation and Controlled Growth for Size Predictable Synthesis of Nanoscale Metal–Organic Frameworks (MOFs): A General and Scalable Approach. *Angewandte Chemie International Edition* **2018**, *57* (26), 7836-7840.
15. Palomba, J. M.; Wirth, D. M.; Kim, J. Y.; Kalaj, M.; Clarke, E. M.; Peterson, G. W.; Pokorski, J. K.; Cohen, S. M., Strong, Ductile MOF–Poly(urethane urea) Composites. *Chemistry of Materials* **2021**, *33* (9), 3164-3171.
16. Zhang, Y.; Yuan, S.; Feng, X.; Li, H.; Zhou, J.; Wang, B., Preparation of Nanofibrous Metal–Organic Framework Filters for Efficient Air Pollution Control. *Journal of the American Chemical Society* **2016**, *138* (18), 5785-5788.
17. Li, Z.; Zhu, Y.-L.; Niu, W.; Yang, X.; Jiang, Z.; Lu, Z.-Y.; Liu, X.; Sun, J., Healable and Recyclable Elastomers with Record-High Mechanical Robustness, Unprecedented Crack Tolerance, and Superhigh Elastic Restorability. *Advanced Materials* **2021**, *33* (27), 2101498.
18. Wang, T.; Deng, H.; Li, N.; Xie, F.; Shi, H.; Wu, M.; Zhang, C., Mechanically strong non-isocyanate polyurethane thermosets from cyclic carbonate linseed oil. *Green Chemistry* **2022**, *24* (21), 8355-8366.

Appendix A

SUPPORTING INFORMATION FOR CHAPTER 2

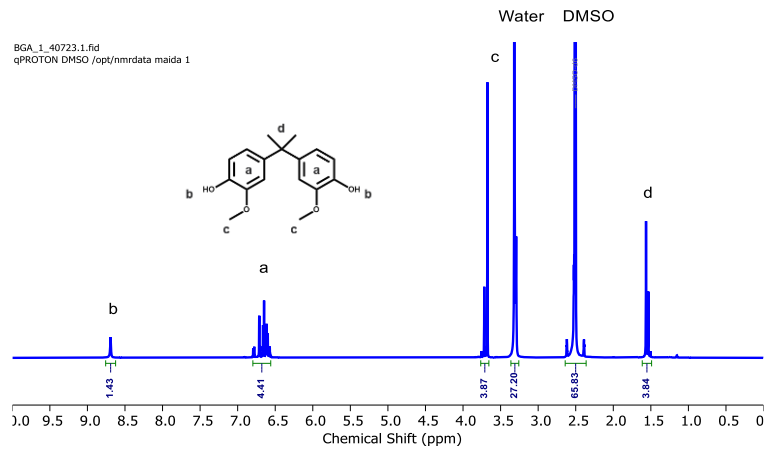


Figure A.1: ^1H NMR spectrum of Bisguaiacol A (BGA).

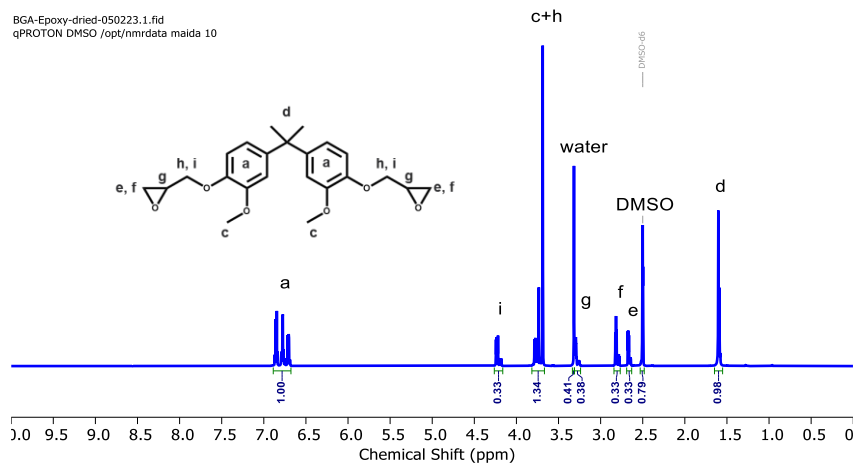


Figure A.2: ^1H NMR spectrum of BGA diglycidyl ether.

BGACC-dry-052623.1.fid
qPROTON DMSO /opt/nmrdata maيدا 2

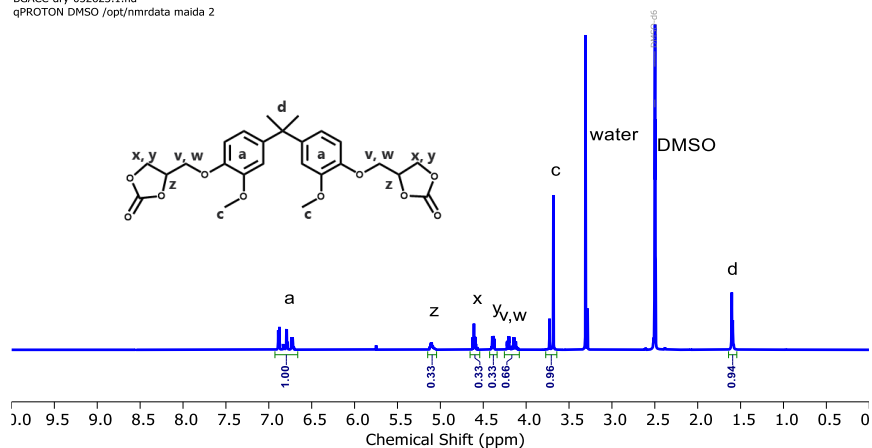


Figure A.3: ^1H NMR spectrum of BGA cyclic carbonate.

BGA-NIPU-washed-061523.1.fid
qPROTON DMSO /opt/nmrdata maيدا 11

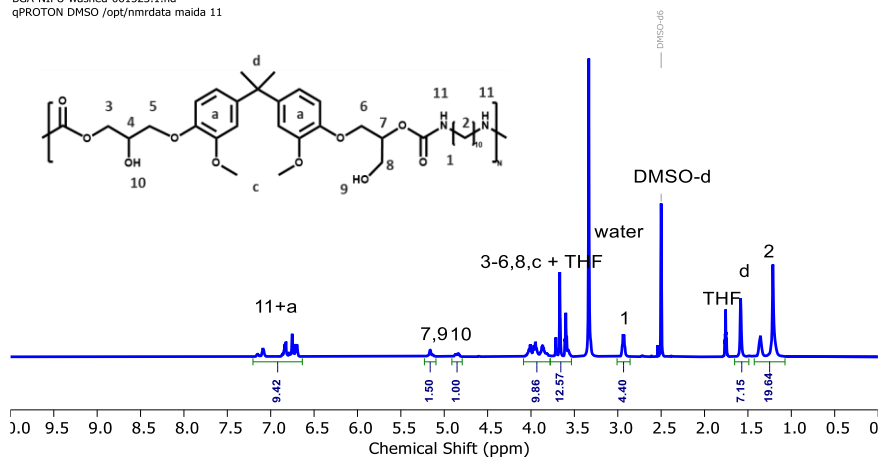


Figure A.4: ^1H NMR spectrum of BGA non-isocyanate polyurethane (NIPU).

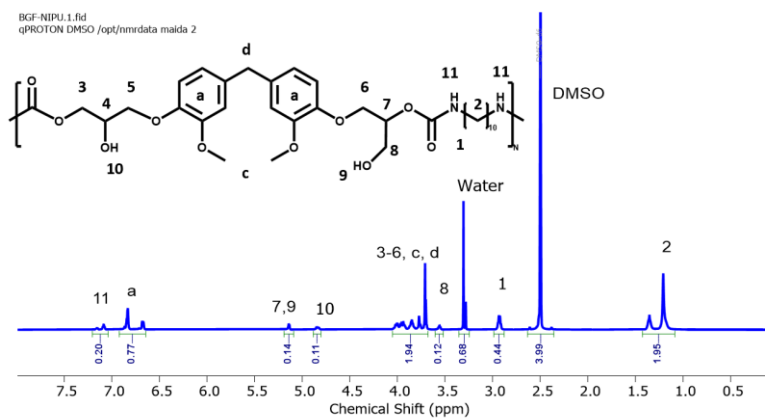


Figure A.5: ^1H NMR spectrum of Bisguaiacol F (BGF) NIPU.

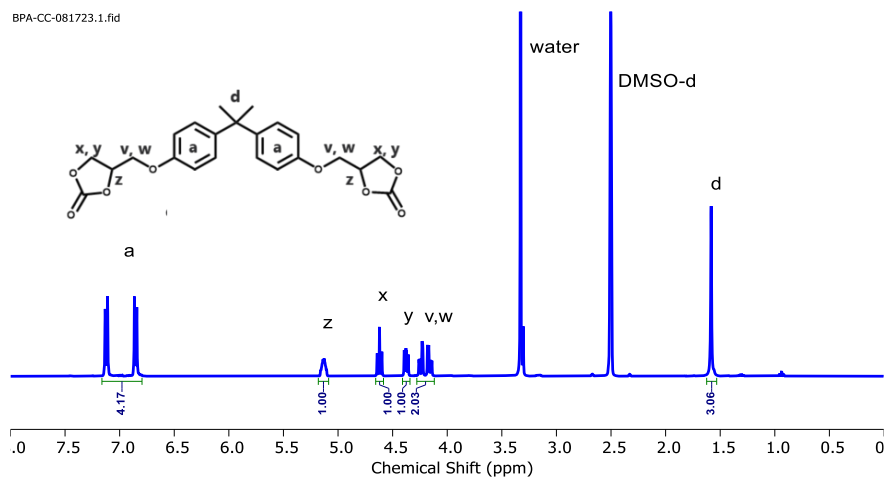


Figure A.6: ^1H NMR spectrum of bisphenol A (BPA) cyclic carbonate.

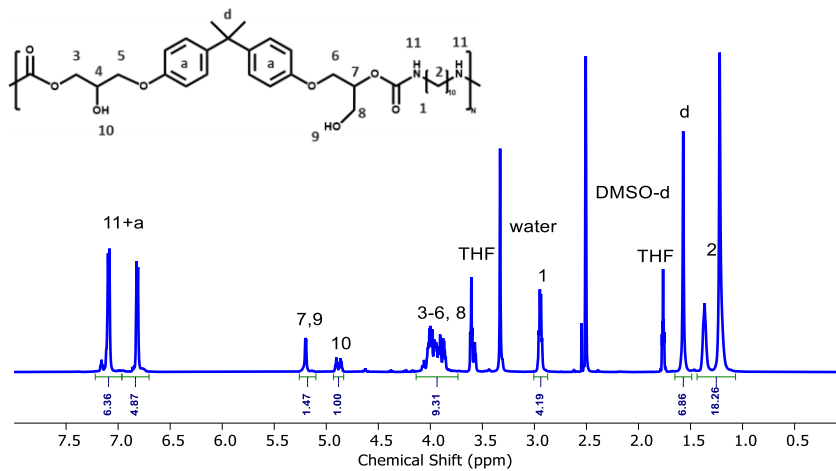


Figure A.7: ¹H NMR spectrum of BPA-NIPU.

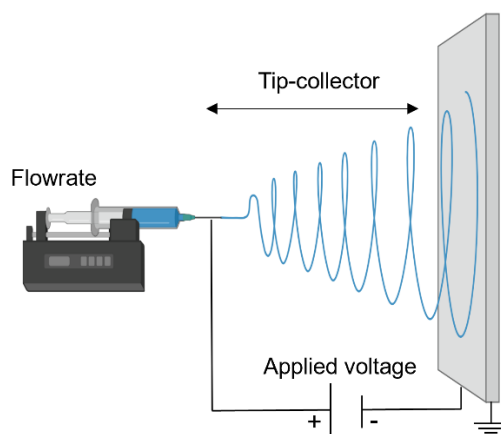


Figure A.8: Schematic representation of the electrospinning setup (created with BioRender).

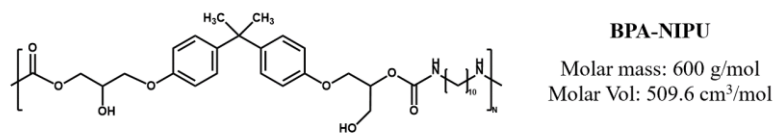
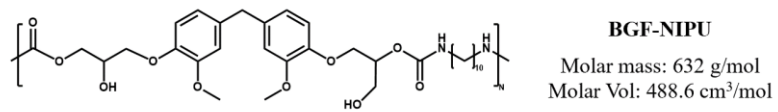
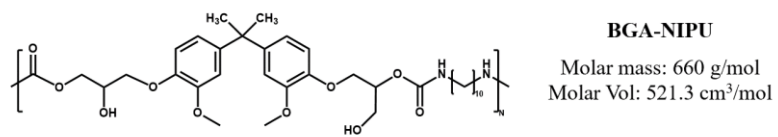


Figure A.9: Repeat units, molar mass and estimated molar volume of BGA-, BGF-, and BPA-NIPUs.

BPA-NIPU		
Structural Group	Van der Walls (VdW) Volume of structural group (cm ³ /mol)	Number of groups
-COO-	15.2	2
-CH2-	10.23	14
-CH(OH)-	14.8	1
-O- (ar.)	-5	2
Para phenyl	43.3	2
-C(CH3)2-	30.7	1
-NH-	4	2
>CH-	6.8	1
OH-	8	1

Structural Group	Number	F _{d,i}	F _{p,i}	E _{h,i}
-CH2-	14	270	0	0
>C<	1	-70	0	0
-CH3	2	420	0	0
-COO-	2	390	490	7000
substituted phenyl ring (o, m, p)	2	1270	110	0
-O-	2	100	400	3000
-NH-	2	160	210	3100
>CH-	2	80	0	0
-OH	2	210	500	20000

VdW volume of repeat unit = 318.5 cm³/mol

Molar Volume of repeat unit = 1.6 * VdW vol. of repeat unit

Molar volume of repeat unit (V) = 509.6 cm³/mol

$$\delta_d = \frac{\sqrt{\sum E_{h,i}}}{V} = 17.6 \text{ (J}\cdot\text{cm}^{-3}\text{)}^{0.5}$$

$$\delta_p = \frac{\sqrt{\sum F_{p,i}^2}}{V} = 2.3 \text{ (J}\cdot\text{cm}^{-3}\text{)}^{0.5}$$

$$\delta_h = \frac{\sqrt{\sum E_{h,i}}}{V} = 11.4 \text{ (J}\cdot\text{cm}^{-3}\text{)}^{0.5}$$

$$\delta_t = \sqrt{\delta_d^2 + \delta_p^2 + \delta_h^2} = 21.1 \text{ (J}\cdot\text{cm}^{-3}\text{)}^{0.5}$$

Figure A.10: Solubility parameter calculations for BPA-NIPU. The values of Van der Walls volume of the structural groups, and the solubility parameter component group contributions (F_{d,i}, F_{p,i}, E_{h,i}) were obtained from the literature.^{1, 2} Molar volume was obtained from the VdW volume as described in the literature.²

BGA-NIPU		
Structural Group	Van der Walls Volume of structural group (cm ³ /mol)	Number of groups
-COO-	15.2	2
-CH2-	10.23	14
-CH(OH)-	14.8	1
-O- (ar.)	-5	4
di-ortho-para-substituted phenyl	38.3	2
-CH3	13.67	2
-C(CH3)2-	30.7	1
-NH-	4	2
>CH-	6.8	1
OH-	8	1

Structural Group	Number	F _{d,i}	F _{p,i}	E _{h,i}
-CH2-	14	270	0	0
>C<	1	-70	0	0
-CH3	4	420	0	0
-COO-	2	390	490	7000
substituted phenyl ring (o, m, p)	2	1270	110	0
-O-	4	100	400	3000
-NH-	2	160	210	3100
>CH-	2	80	0	0
-OH	2	210	500	20000

VdW volume of repeat unit = 325.9 cm³/mol

Molar Volume of repeat unit = 1.6 * VdW vol. of repeat unit

Molar volume of repeat unit = 521.4 cm³/mol

$$\delta_d = \frac{\sqrt{\sum E_{h,i}}}{v} = 19.2 \text{ (J}\cdot\text{cm}^{-3}\text{)}^{0.5}$$

$$\delta_p = \frac{\sqrt{\sum F_{p,i}^2}}{v} = 2.5 \text{ (J}\cdot\text{cm}^{-3}\text{)}^{0.5}$$

$$\delta_h = \frac{\sqrt{\sum E_{h,i}}}{v} = 11.8 \text{ (J}\cdot\text{cm}^{-3}\text{)}^{0.5}$$

$$\delta_t = \sqrt{\delta_d^2 + \delta_p^2 + \delta_h^2} = 22.7 \text{ (J}\cdot\text{cm}^{-3}\text{)}^{0.5}$$

Figure A.11: Solubility parameter calculations for BGA-NIPU. The values of Van der Walls volume of the structural groups, and the solubility parameter component group contributions (F_{d,i}, F_{p,i}, E_{h,i}) were obtained from the literature.^{1,2} Molar volume was obtained from the VdW volume as described in the literature.²

BGF-NIPU		
Structural Group	Van der Walls Volume of structural group (cm ³ /mol)	Number of groups
-COO-	15.2	2
-CH2-	10.23	15
-CH(OH)-	14.8	1
-O- (ar.)	-5	4
di-ortho-para-substituted phenyl	38.3	2
-CH3	13.67	2
-NH-	4	2
>CH-	6.8	1
OH-	8	1

Structural Group	Number	$F_{d,i}$	$F_{p,i}$	$E_{h,i}$
-CH2-	15	270	0	0
-CH3	2	420	0	0
-COO-	2	390	490	7000
substituted phenyl ring (o, m, p)	2	1270	110	0
-O-	4	100	400	3000
-NH-	2	160	210	3100
>CH-	2	80	0	0
-OH	2	210	500	20000

VdW volume of repeat unit = 305.4 cm³/mol

Molar Volume of repeat unit = 1.6 * VdW vol. of repeat unit

Molar volume of repeat unit = 488.6 cm³/mol

$$\delta_d = \frac{\sqrt{\sum E_{h,i}}}{v} = 19.5 \text{ (J}\cdot\text{cm}^{-3}\text{)}^{0.5}$$

$$\delta_p = \frac{\sqrt{\sum F_{p,i}^2}}{v} = 2.7 \text{ (J}\cdot\text{cm}^{-3}\text{)}^{0.5}$$

$$\delta_h = \frac{\sqrt{\sum E_{h,i}}}{v} = 12.2 \text{ (J}\cdot\text{cm}^{-3}\text{)}^{0.5}$$

$$\delta_t = \sqrt{\delta_d^2 + \delta_p^2 + \delta_h^2} = 23.1 \text{ (J}\cdot\text{cm}^{-3}\text{)}^{0.5}$$

Figure A.12: Solubility parameter calculations for BGF-NIPU. The values of Van der Walls volume of the structural groups, and the solubility parameter component group contributions ($F_{d,i}$, $F_{p,i}$, $E_{h,i}$) were obtained from the literature.^{1,2} Molar volume was obtained from the VdW volume as described in the literature.²

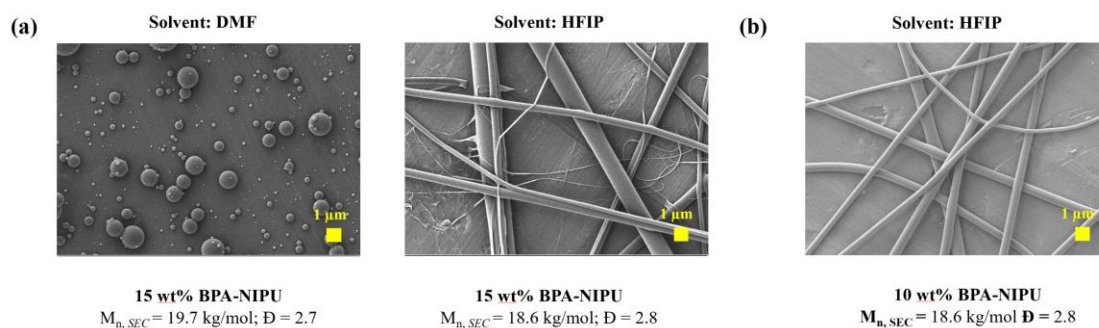


Figure A.13: Initial electrospinning trials with BPA-NIPU. (a) HFIP produced fibers (diameter = $986 \pm 704 \text{ nm}$); DMF-based solution only produced beads. (b) BPA-NIPU spun at $\sim 10\%$ w/v in HFIP produced sub-micron fiber (fiber diameter = $470 \pm 203 \text{ nm}$). Process conditions for the trials: flowrate = 0.5 ml/h ; tip-collector distance = 15 cm ; voltage = $5\text{-}6 \text{ kV}$; Needle size = 18 G .

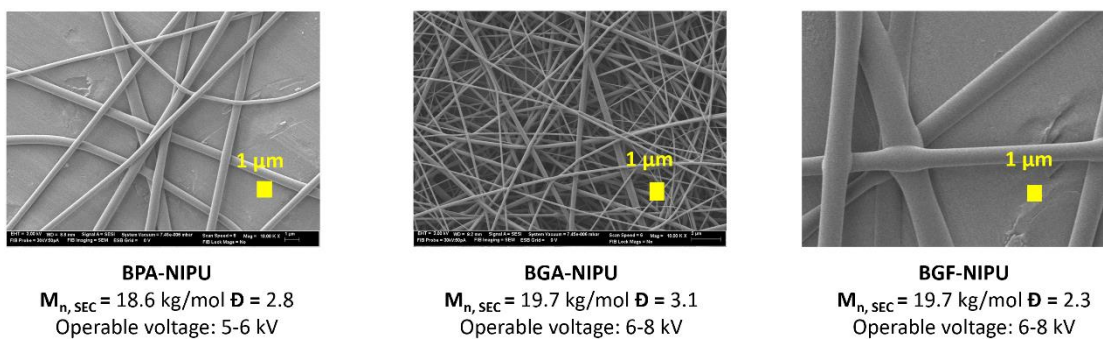


Figure A.14: BPA-, BGA-, and BGF-NIPUs electrospun at $\sim 10\%$ w/v in HFIP at fixed flow rate (0.5 ml/h), tip-to-collector distance (15 cm), and needle diameter (18 G) to determine the operable voltage window.

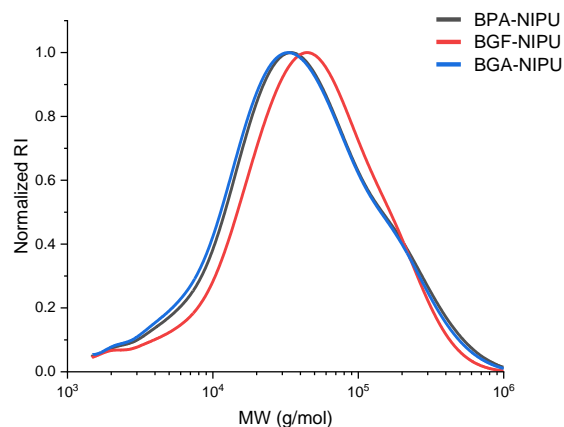


Figure A.15: SEC chromatograms for BPA-, BGA-, and BGF-NIPUs in DMAc/LiBr (0.5% w/w) using PMMA standards.

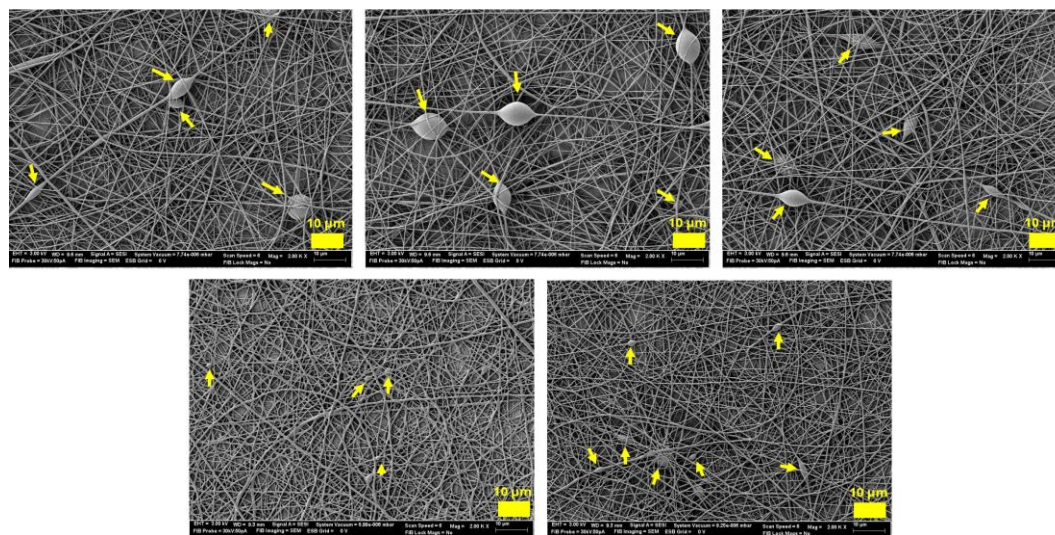


Figure A.16: Electrospun fiber mats of 10% w/v BPA-NIPU in HFIP. Arrows indicating bead formation. The number of beads was averaged for 5 images at 2000 X magnification, revealing 5 ± 1 beads per $7844 \mu\text{m}^2$.

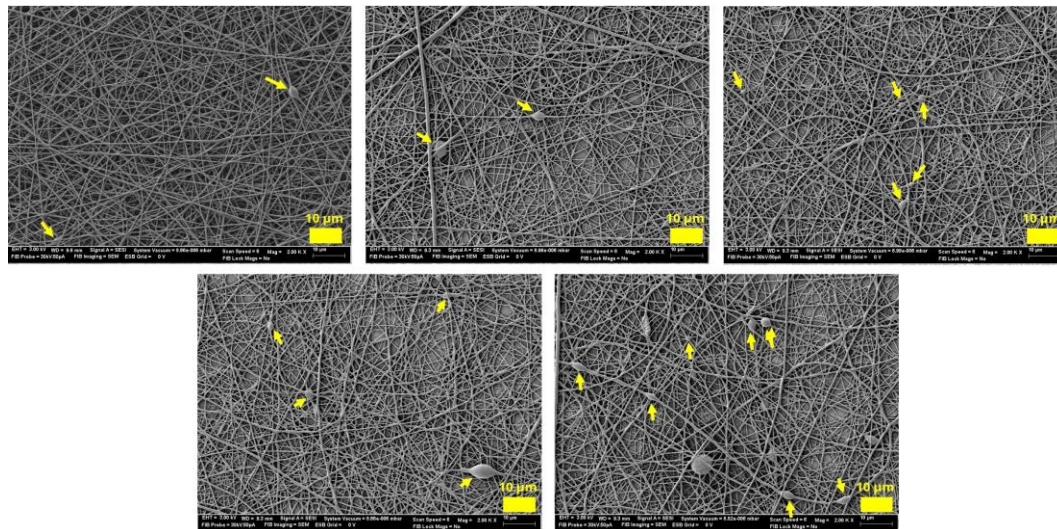


Figure A.17: Electrospun fiber mats of 10% w/v BGA-NIPU in HFIP. Arrows indicating bead formation. The No. of beads was averaged for 5 images at 2000 X magnification, revealing 4 ± 2 beads per $7844 \mu\text{m}^2$.

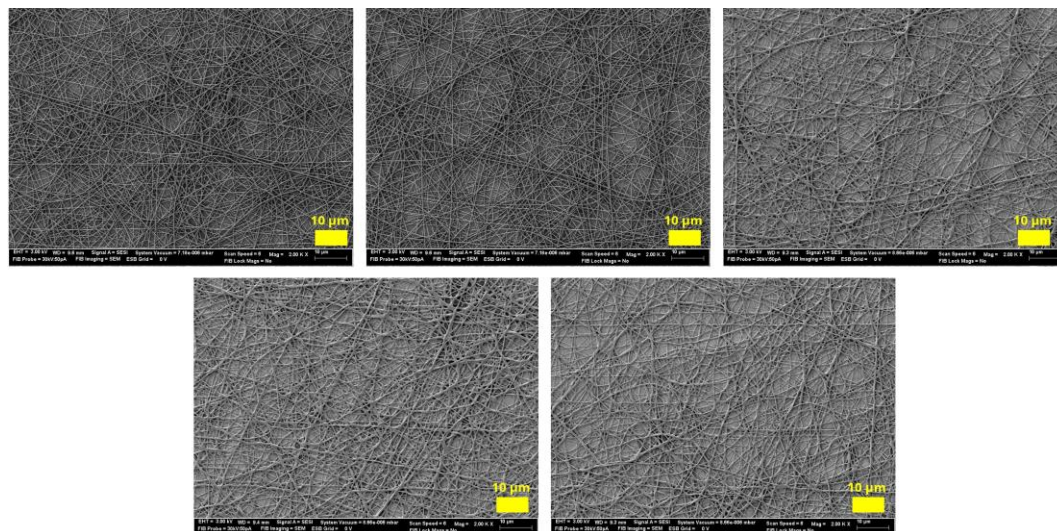


Figure A.18: Electrospun fiber mats of 10% w/v BGF-NIPU in HFIP. Arrows indicating bead formation. No beads were found in this sample as shown in the 2000 X magnification images.

Appendix B

SUPPORTING INFORMATION FOR CHAPTER 3

B.1 Preparation of Cu-BTC

A 7.5 mM solution of copper acetate monohydrate in DMF/EtOH (3:1) was heated to 45 °C in a 50-mL, three-necked, round bottom flask equipped with a magnetic stir bar. Next, metal stock solution (150 mM of copper acetate monohydrate in DMF/EtOH (1:1)) and ligand stock solution (150 mM of trimesic acid in DMF) simultaneously were pumped, using programmable syringe pump (Braintree Scientific BS-8000), into the reaction flask at 38 ml/h under constant stirring at 500 rpm. The reaction mixture changed color from green blue of copper salt to cyan blue of Cu-BTC almost instantaneously. The reaction mixture was then cooled to 25 °C followed by centrifugation and decanting of the supernatant. The resulting MOF crystals were washed with DMF (2x) and EtOH (2x) and dried at 130 °C for 24 h under vacuum (Fisherbrand Isotemp Model 281A vacuum oven, Fisherbrand MaximaDry diaphragm vacuum pump).

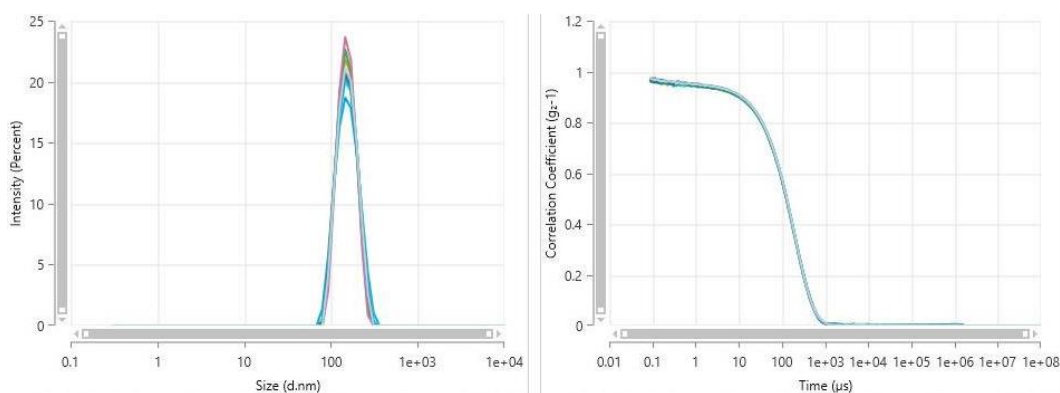


Figure B.1: DLS plot of Cu-BTC in DMF (~1 mg/mL). Z Avg. = 149 ± 1 nm; PDI = 0.05 ($PDI = [SD/Mean]^2$)³. Averaged for nine measurements.

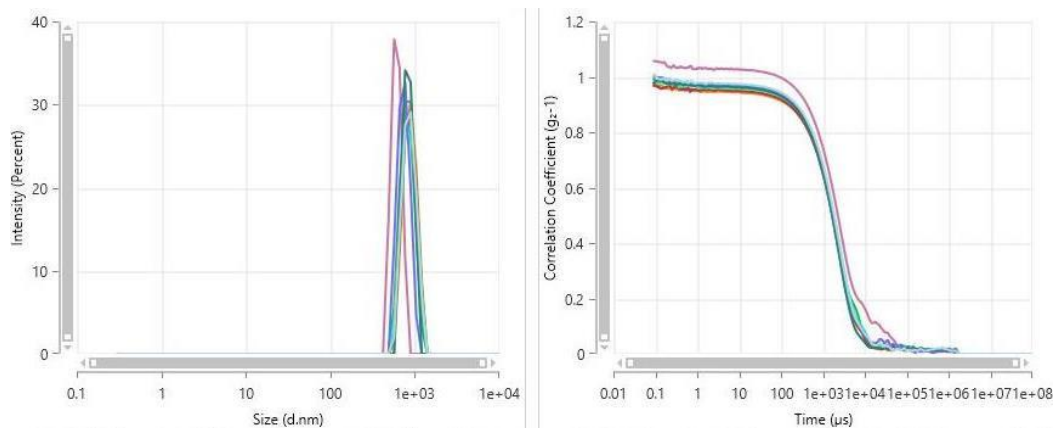


Figure B.2: DLS plot of Cu-BTC in HFIP (~1 mg/mL). Z Avg. = 840 ± 54 nm; PDI = 0.21 ($PDI = [SD/Mean]^2$)³. Averaged for nine measurements.

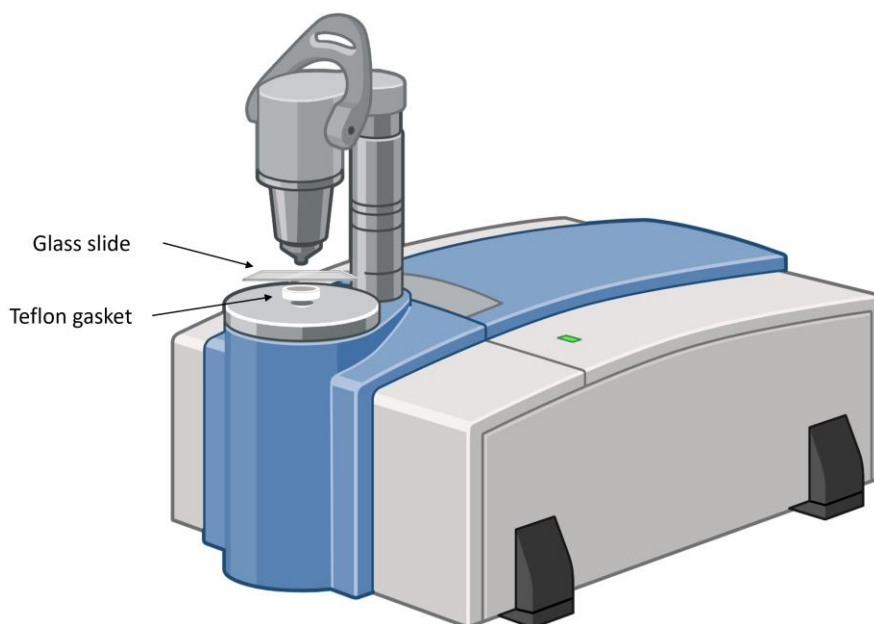


Figure B.3: Schematic representation of the ATR-FTIR setup used (image created using BioRender). A Teflon gasket was placed around the ATR crystal, and the sample was poured into the gap on top of the crystal. Next, the gap was covered by a glass slide to minimize solvent evaporation during testing.

REFERENCES

1. Van Krevelen, D. W.; Te Nijenhuis, K., Chapter 7 - Cohesive Properties and Solubility. In *Properties of Polymers (Fourth Edition)*, Van Krevelen, D. W.; Te Nijenhuis, K., Eds. Elsevier: Amsterdam, 2009; pp 189-227.
2. Van Krevelen, D. W.; Te Nijenhuis, K., Chapter 4 - Volumetric Properties. In *Properties of polymers (Fourth Edition)*, Van Krevelen, D. W.; Te Nijenhuis, K., Eds. Elsevier: Amsterdam, 2009; pp 71-108.
3. Nobbmann, U. Polydispersity – what does it mean for DLS and chromatography? <https://www.materials-talks.com/polydispersity-what-does-it-mean-for-dls-and-chromatography/> (accessed November 15).